ARTICLE

https://doi.org/10.1590/2317-4889202320220092

BJGEO
Brazilian Journal of Geology

Mineral chemistry from the Alfeu-I lamproite (Southern Brazil) and its contribution to understand the mantle heterogeneity under South American Plate during the Gondwana breakup

Larissa Colombo Carniel[1]*, Rommulo Vieira Conceição[1,2], Carlos Augusto S. Provenzano[3], Andrea Sander[3], Felipe Padilha Leitzke[4], Andrea Brum da Silva[2], Jasper Berndt[5], Stephan Klemme[5]

Abstract

The Alfeu-I lamproite is one of the few alkaline rock occurrences in the South of Brazil that represents the alkaline event related to the South Atlantic opening and the enormous magmatic activity that formed the Paraná basalts. Alfeu-I lamproite is a diatreme facies and exhibits an inequigranular texture with macrocrysts of mica, spinel, garnet, and ilmenite and microcrysts of mica, pyroxene, and rare olivine, all immersed in a groundmass of pyroxene, spinel, perovskite, rutile, ilmenite, and, more rarely, olivine. Major element compositions of Alfeu-I pyroxene, garnet, ilmenite, mica, and olivine were determined by electron microprobe analyses, and trace element concentrations of clinopyroxene, garnet, ilmenite, and mica were measured using laser-ablation inductively coupled plasma mass spectrometry techniques. Temperature, pressure, and oxygen fugacity (fO_2) conditions during the crystallization of Alfeu-I lamproite were calculated with the geothermobarometers and olivine, spinel, garnet, and orthopyroxene. The resulting mean equilibrium temperature ranges from 1375°C at 4 GPa to 1395°C at 5 GPa, whereas the fO_2 points to $\Delta FMQ = +2.4$ (at 4 GPa) and $\Delta FMQ = +2.2$ (at 5 GPa). Rb-Sr and Sm-Nd isotopic data together with the trace element concentrations of minerals suggest that melting of a mantle source enriched in incompatible elements and volatiles due to previous subduction events occurred during the Gondwana breakup around 125 Ma ago. Fluids that may have originated from subducting slabs in the old subduction zone are probably the cause of the high fO_2 conditions in Alfeu-I lamproite.

KEYWORDS: Gondwana sub-lithospheric mantle; mineral chemistry; lamproite; mantle redox conditions.

INTRODUCTION

Lamproites are formed by partial melting of metasomatized lithospheric mantle (Scott Smith *et al.* 2018) and are usually classified according to the mineralogical and geochemical criteria given by Mitchell and Bergman (1991). However, the name lamproite was recently redefined by Scott Smith *et al.* (2018) to emphasize the common petrogenesis and eliminate petrological confusion with petrogenetically distinct kimberlite. Although they are volumetrically minor components of continental magmatism, lamproites are rare products of the melting of geochemically exceptional and variable lithospheric mantle sources. Mitchell (1995) underlined that kimberlites and related rocks cannot be identified only by petrography and that geochemical data are scant due to metasomatism, crustal contamination, and, perhaps most important, weathering. The best studied material for rock classification is obtained from the hypabyssal facies of these rocks, since they contain less crustal xenoliths and the minerals are well crystallized to allow a better understanding of the primary mineral assemblage. Classification based on whole rock chemistry of diatreme facies, as in the case of Alfeu-I lamproite, is more difficult because of the predominance of fragmented lapilli and the tendency of these rocks to weathering. In this case, mineral chemistry and *in situ* isotope characterization provide a better contribution to the understanding of the origin and magmatic history of the lamproite rocks.

The Alfeu-I lamproite, located in the southeastern portion of the Sul-Riograndense Shield, southern Brazil, is one of the

Supplementary data

Supplementary data associated with this article can be found in the online version: http://sfbjg.siteoficial.ws/Sf/2023/415220220092.pdf

[1]Laboratório de Geoquímica e Petrologia Experimental, Universidade Federal do Rio Grande do Sul – Porto Alegre (RS), Brazil. E-mails: larissa.colombo@ufrgs.br; rommulo.conceicao@ufrgs.br

[2]Programa de Pós-Graduação em Geociências, Universidade Federal do Rio Grande do Sul – Porto Alegre (RS), Brazil. E-mail: geo_abrum@hotmail.com

[3]Geological Survey of Brazil – Porto Alegre (RS), Brazil. E-mail: carlos.provenzano@cprm.gov.br; andrea.sander@cprm.gov.br

[4]Centro de Engenharias, Universidade Federal de Pelotas – Pelotas (RS), Brazil. E-mail: felipe.leitzke@ufpel.edu.br

[5]Institut für Mineralogie, Westfälische Wilhelms-Universität Münster – Münster, Germany. E-mails: stephan.klemme@uni-muenster.de; jberndt@uni-muenster.de

*Corresponding author.

rare occurrences of alkaline rocks that may further our understanding of the magma diversity production during the opening of the South Atlantic. There is scarce information on the petrogenesis of alkaline rocks from this part of Brazil, and no detailed studies of the trace element geochemistry and Sr-Nd isotope compositions of these rocks have been published.

Pressure, temperature, and redox conditions (fO_2) of lamproites and related rocks provide valuable insights on the mantle source and the melting regime of these rocks. However, the application of geothermobarometers and oxygen barometers in lamproites and related rocks is difficult due to the mostly low preservation grade of these rocks, which is usually the main obstacle, but also due to the diversified mineral assemblage, which sometimes does not contain all the minerals required for geothermobarometric calculations. In this study, we use pyroxene, garnet, ilmenite, mica, and olivine compositions to determine age, temperature, pressure, and fO_2 conditions for the Alfeu-I lamproite to constrain its mantle source and the geological context related to the Atlantic opening. Moreover, we also use these new data to infer the potential of these melts to carry and preserve diamonds.

GEOLOGICAL SETTINGS AND SAMPLES

Alfeu-I lamproite is a volcanic pipe emplaced in the Pinheiro Machado Suite of the Pelotas Batholith domain and occurs in the eastern portion of the Sul-Riograndense Shield, southern Brazil. Its location is around 300 km from the Rosário-6 alnöite and the Paraná basalts (Fig. 1). The alkaline rocks in this region occurred in four main stages: Permian to Triassic, probably caused by the stress propagation related to the Cabo La Ventana orogeny (Gomes *et al.* 1996, Milani 1997); lower Cretaceous, associated with the rifting of the Atlantic marginal basin; upper Cretaceous, contemporaneous to the Atlantic

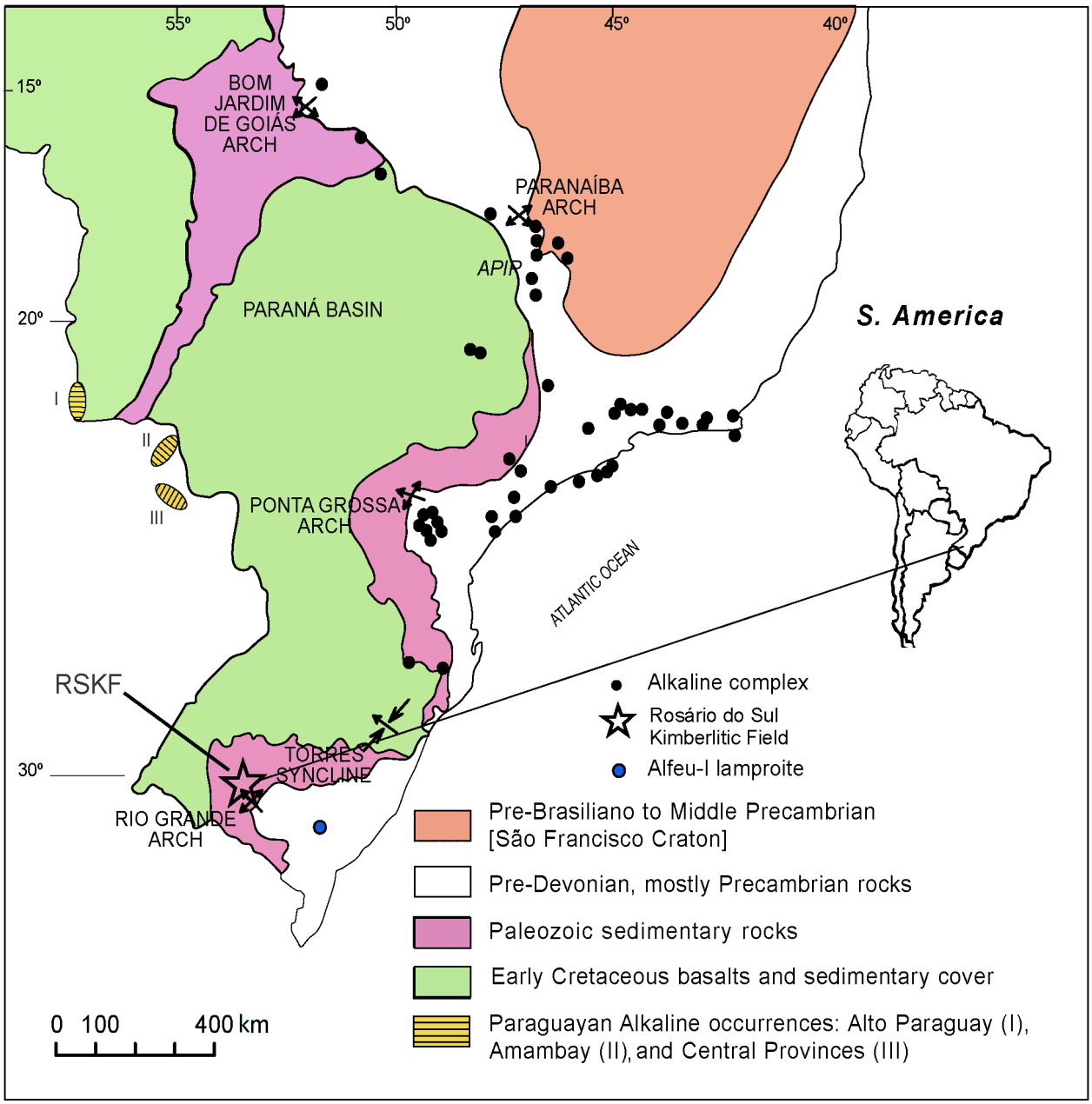

Figure 1. Simplified geological map of the Alfeu-I lamproite based on Svisero and Chieregati (1991), Conceição *et al.* (2019), Morbidelli *et al.* (2000), and Carniel *et al.* (2020). Río de la Plata Craton limit from Santos *et al.* (2019).

Ocean; and Cenozoic (Paleogene), linked to the evolution of continental rift systems in southeastern Brazil (Ribeiro 1980, Almeida 1983). The Mesozoic alkaline magmatism is conditioned by shear zones and discontinuities between cratonic limits that were reactivated by the Gondwana breakup tectonics (Barbieri *et al*. 1987, Gomes and Comin-Chiaramonti 2017).

The Alfeu-I rocks overlap the Canguçu Dorsal Transcurrent Shear Zone, intruded into granodioritic to monzogranitic orthogneisses from the Pinheiro Machado Granite-Gneiss Complex (780–610 Ma) (Fragoso-César 1991, Philipp 1991) (Fig. 2A). The samples are quite weathered (Fig. 2B); however, it is possible to identify preserved minerals and the original texture in thin sections. These rocks are composed of macrocrysts and microcrysts (pyroxene, garnet, spinel, ilmenite, biotite, and olivine) in an interstitial matrix with some imbricated pelletal lapilli, wall rock autoliths, and crustal xenoliths.

METHODS

The Alfeu-I minerals were selected with a binocular magnifying glass from the pan-concentrate that was collected from the altered rock. Microprobe analyses were performed on mineral separates of pyroxene, garnet, ilmenite, mica, and olivine macrocrysts (> 0.5–10 mm) and microcrysts (< 0.5 mm) using a CAMECA SX-five electron microprobe of the Laboratório de Microssonda Eletrônica (CPGq-IG/UFRGS), Brazil. The analyses were performed using an acceleration voltage of 15 kV, a beam current of 10 nA, a beam size of 5 µm, and a counting time of 20 s on the peak and 5 s on each background. The standards used included sanidine (Si, Al), diopside (Mg, Ca), almandine (Fe), rutile (Ti), chromium oxide (Cr), and rhodonite (Mn). Details of the method are given in the *Supplementary data*. The fresh minerals were analyzed in the core and border, whereas the ones more altered were analyzed just in the core, as we pointed out in the Suppl. Data.

Trace element concentrations of the Alfeu-I minerals (clinopyroxene, garnet, biotite, and ilmenite) were determined with laser-ablation inductively coupled plasma mass spectrometry (LA-ICP-MS) at the Institut für Mineralogie, Münster, Germany (Beyer *et al*. 2013, Wijbrans *et al*. 2015). Sample ablation was performed with a pulsed 193 nm ArF excimer laser (Analyte G2, Photon Machines). A repetition rate of 5 or 10 Hz and an energy of ~3–4 J/cm^2 were used. The beam spot diameter varied between 15 and 30 µm. Elemental analysis has been carried out with an Element XR mass spectrometer (ThermoFisher Scientific). Forward power was 1300 W and reflected power was < 1 W; gas flow rates were about 1 L/min for He (carrier gas of ablated material), 0.8 L/min for the Ar-auxiliary gas, and 1 L/min for the sample gas, respectively. The cooling gas flow rate was set to 16 L/min. Before starting analysis, the system has been tuned on a NIST 612

Figure 2. (A) Alfeu-I lamproite emplaced in the Pinheiro Machado Suite of the Pelotas Batholith domain; (B) Alfeu-I weathered samples (Provenzano 2016).

reference glass measuring ^{139}La, ^{232}Th, and $^{232}Th^{16}O$ to get stable signals and high sensitivity, as well as low oxide production rates ($^{232}Th^{16}O/^{232}Th < 0.1\%$) during ablation. A total of 32 elements were quantitatively analyzed. Masses monitored were ^{7}Li, ^{29}Si, ^{43}Ca, ^{51}V, ^{53}Cr, ^{55}Mn, ^{59}Co, ^{60}Ni, ^{61}Ni, ^{63}Cu, ^{66}Zn, ^{69}Ga, ^{72}Ge, ^{73}Ge, ^{85}Rb, ^{88}Sr, ^{89}Y, ^{90}Zr, ^{93}Nb, ^{118}Sn, ^{121}Sb, ^{133}Cs, ^{137}Ba, ^{139}La, ^{140}Ce, ^{141}Pr, ^{146}Nd, ^{147}Sm, ^{153}Eu, ^{157}Gd, ^{159}Tb, ^{163}Dy, ^{165}Ho, ^{166}Er, ^{169}Tm, ^{172}Yb, ^{175}Lu, ^{178}Hf, ^{181}Ta, ^{182}W, ^{208}Pb, ^{232}Th, and ^{238}U. The NIST 612 glass was used as an external reference material and ^{29}Si, ^{43}Ca (silicates), ^{47}Ti (Fe-Ti oxides), and ^{26}Mg (spinels) as internal standards, which have been previously determined by electron microprobe. The overall time of a single analysis was 75 s (20 s for background, 40 s for peak after switching the laser on, 15 s washout time). Concentrations of measured elements were calculated using the Glitter software (Van Achterbergh *et al.* 2001, Griffin *et al.* 2008). Standard reference glasses BCR2-G and BIR1-G were analyzed as monitors for precision and accuracy for silicate phases of this study. Standard analyses were repeated every 20 analyses of unknown minerals (Suppl. Data). The obtained results match the published range of concentrations given in the GeoReM database (version 18) (Jochum *et al.* 2005).

Rb-Sr and Sm-Nd isotopic analyses were performed using two different thermal ionization mass spectrometers (Sector 54, VG Scienta Holdings AB; and Triton, ThermoFisher Scientific) for isotopic characterization at the Laboratório de Geologia Isotópica (LGI-IG, UFRGS), Brazil. Around 0.5–0.8 g of each mineral was crushed in an agate mortar and leached with HCl 0.1 N in order to eliminate the crustal alteration. Posteriorly, 0.1 g of the leached residue was spiked with mixed $^{87}Rb/^{84}Sr$ and $^{149}Sm/^{150}Nd$ tracers and then digested with HF, HNO_3, and HCl until complete dissolution, followed by drying and homogenization of the residue in 3 mL of HCl 2.5N. Columns filled with cationic AG-50W-X8 (200–400 mesh) and anionic LN-B50-A (100–150 mesh) resins were used to separate Rb, Sr, and REE and Sm, Nd, respectively. Each sample was dried to a solid residue and then loaded with 0.25N H_3PO_4 in appropriate filaments (single Ta filaments for Rb, Sr, Sm, and triple Ta–Re–Ta for Nd). Sr and Nd isotopic ratios were normalized to $^{86}Sr/^{88}Sr=0.1194$ and to $^{146}Nd/^{144}Nd = 0.7219$. Measurements of specific standards were performed for accurate analysis. The NIST standard NBS-987 resulted in $^{87}Sr/^{86}Sr = 0.710260 \pm 0.000014$, and the JNd-1 standard resulted in a ratio of $^{143}Nd/^{144}Nd = 0.512108 \pm 0.000010$. Blanks were < 60 pg for Sr, < 500 pg for Rb, < 200 pg for Sm, and < 500 pg for Nd. The errors do not exceed more than 1% of the reported value.

To determine the crystallization temperature and fO_2 of Alfeu-I, we used the olivine-spinel oxygen geothermobarometers of O'Neill and Wall (1987) and Ballhaus *et al.* (1991). The pressure of Alfeu-I was also calculated with the garnet-orthopyroxene geothermobarometer of Nickel and Green (1985). The Fe^{2+} and Fe^{3+} contents of minerals were calculated with the method of Droop (1987), based on stoichiometric criteria. We used analyses of Alfeu-I lamproite from mineral separates, as the Alfeu-I pipe is unfortunately very altered and it was not possible to collect cohesive samples.

RESULTS

Petrography and mineral compositions

The Alfeu-I lamproite rocks exhibit an inequigranular texture with macrocrysts (> 0.5–10 mm) and microcrysts (< 0.5 mm) of biotite (~25 vol%), spinel (~10 vol%), garnet (~5 vol%), and ilmenite (~5 vol%), microcrysts of pyroxene (~3 vol%), and rare olivine (~2 vol%), all immersed in a groundmass (~35 vol%) composed of pyroxene, chromite, perovskite, rutile, ilmenite, and, more rarely, olivine. Perovskite and rutile were identified by MEV-EDS in the Alfeu-I thin sections, but not found in rock concentrates. The macrocrysts and microcrysts are fractured and show corroded edges. Macrocrysts and microcrysts of biotite have curved cleavage planes that indicate the flow orientation and rounded edges (Fig. 3A). Garnet macrocrysts and microcrysts are rounded and fractured, with corroded edges, and they are surrounded by mica (Fig. 3B). Groundmass spinel and perovskite are rare (Figs. 3C and 3D), whereas clinopyroxene is also found in the pelletal lapilli (Figs. 3E and 3F). Olivine is rare and appears only as a serpentine pseudomorph and found also in pelletal lapilli (Fig. 3G). Xenoliths from the wall rock are rare, but two of them were observed in thin sections with an angular sub-rounded shape, from 1 to 3 mm in size, and with granitic composition. Xenocrysts consisting of polycrystalline quartz, microcline, and rare plagioclase are also present and occur with rounded shapes and well-defined edges, up to 1 mm in diameter. These xenocrysts are found aligned with the flow texture (Fig. 3H). Due to the lack of fresh rock in the Alfeu-I lamproite, we need to consider that all minerals underwent secondary alteration, and this open-system process produced changes in the mineral composition, as we will discuss below. The xenoliths, xenocrysts, and lapilli compose ~15 vol% of the rock.

Pyroxene

Pyroxene microcrysts are classified as augite ($(Al_{0.2}Ti_{0.03}Fe_{0.32}Mn_{0.004}Mg_{0.58}Ca_{0.62}Na_{0.26})_{2.01}(Si_{1.94}Al_{0.06})_2O_6$ on the basis of 6 oxygens) and enstatite ($(Al_{0.03}Ti_{0.003}Fe_{0.17}Mn_{0.003}Mg_{1.74}Ca_{0.03}Na_{0.01})_{1.98}(Si_{1.9}Al_{0.1})_2O_6$ on the basis of 6 oxygens) (Fig. 4; Suppl. Data). Enstatites have SiO_2 contents of 54–56 wt.%, Al_2O_3 contents of 3–4.4 wt.%, MgO of 32–35 wt.%, MnO up to 0.15 wt.%, Cr_2O_3 contents of 0.39–0.86 wt.%, Na_2O contents up to 0.17 wt.%, and Mg# ((100*Mg)/(Mg+Fe)) of 88–93, whereas augites have CaO contents ranging from 15 to 16 wt.%, Al_2O_3 contents of 4.8–6.6 wt.%, MgO from 9 to 11 wt.%, Na_2O contents of 3.2–4 wt.%, Mg# of 58–68, and Ca# of 49–54. Augites also have lower Cr_2O_3 contents than enstatites, up to 0.06 wt.%, and similar MnO contents, from 0.1 to 0.18 wt.%.

Figure 5A ($Cr_2O_3 \times Al_2O_3$ and Cr × Fe × Na molar) shows that Alfeu-I clinopyroxenes plot in the eclogites and Cr-poor megacrysts field and Alfeu-I orthopyroxenes in APIP field, which is the field of peridotite nodules in Alto Paranaíba Province. In Fig. 5B (Mg# × Ca#), Alfeu-I clinopyroxenes plot with lower Mg# and higher Ca# than pyroxene from lherzolites, wehrlites, PIC, and MARID rocks. Trace element contents of clinopyroxenes have homogeneous composition,

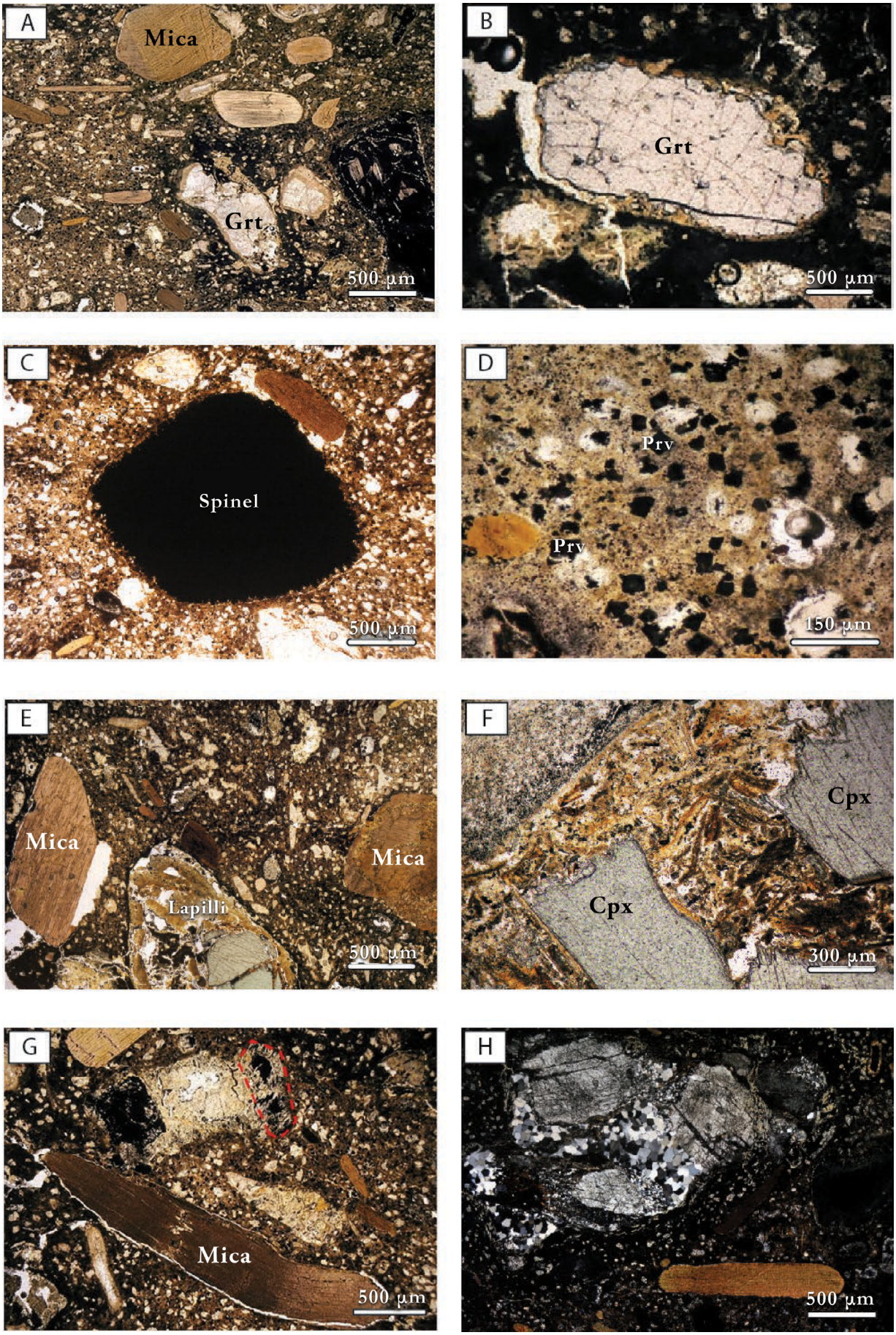

Figure 3. Microscope features of the Alfeu-I rocks: (A, B) uncrossed polarized image of fragments of clinopyroxene (Cpx) in pelletal lapilli (B is a detail of A); (C, D) uncrossed polarized image of large spinel and small perovskite (Prv) grains of the groundmass; (E) uncrossed polarized image of macrocryst of garnet (Grt) with corroded edges; (F) uncrossed polarized image of the flow orientation indicated by mica microcrysts; (G) uncrossed polarized image of pseudomorphs of olivine outlined in red; (H) crossed polarized image of granite xenolith with polycrystalline quartz.

and the content for V, Sr, and Zr in augites ranges from 213 to 326 ppm, from 91 to 142 ppm, and from 103 to 269 ppm (*Supplementary data*), respectively. Figure 6A shows that Ca content in orthopyroxenes increases with the increase of alkalis, whereas Fig. 6B shows that Ca content in clinopyroxenes increases with the decrease of Mg. Figure 7A shows chondrite normalized (McDonough and Sun 1995) trace element patterns for clinopyroxenes, with positive anomalies of V, Sr, Y, and Zr, negative anomalies of Ni, Nb, and Pb, and an almost flat REE pattern, with only a slight enrichment of HREE relative to LREE (Fig. 7A).

Garnet

Alfeu-I garnets macrocrysts and microcrysts ($(Mg_{4.44}Fe^{2+}_{0.85}Mn_{0.04}Ca_{0.78})_{6.1}(Al_{3.67}Ti_{0.02}Fe^{3+}_{0.06}Cr_{0.24})_{3.99}(Al_{0.01}Si_{6})_{6.0}O_{12}$ on basis of 24 oxygens) are classified as Cr-pyrope (*Supplementary data*), which are typical in peridotites, kimberlites, and lamproites (Mitchell 1995). They are homogeneous, Mg-rich, close to the end-member Pyrope ($Mg_3Al_2Si_3O_{12}$) (Fig. 8). The diagrams Ca/(Ca+Mg) versus Mg/(Mg+Fe) molar and Cr_2O_3 versus CaO (wt.%) (after Schulze 2003) show that the garnet grains have compositions similar to mantle-derived garnets (Figs. 9A and 9B). The garnets have MgO contents of 20–22 wt.%, Al_2O_3 of 21–23 wt.%, Cr_2O_3 of 1–4 wt.%, and MnO of 0.2–0.4 wt.%. Trace element contents in garnets are very homogeneous and the content of V ranges from 104 to 223 ppm and Ni from 54 to 90 ppm (Suppl. Data), whereas the trace element patterns (normalized to chondrite) show positive anomalies of V, Cr Mn, Y, and Zr, and negative anomalies of Ni, Sr, Nb, La, Ce, W, and Th (Fig. 7B).

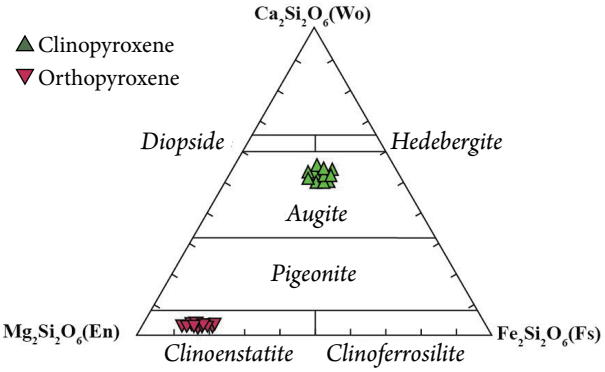

Figure 4. Alfeu-I pyroxenes classified based on the Wo-En-Fs ternary, compiled after Morimoto *et al.* (1988).

Ilmenite

Alfeu-I macrocryst and microcryst ilmenites are ubiquitous, with MgO contents of 0.36–4.9 wt.%, FeO of 42–47 wt.%, TiO_2 of 47–50 wt.%, and MnO contents of 0.2–0.6 wt.% (Suppl. Data). However, seven analyses of four microcryst grains showed higher MnO contents (from 0.62 to 4.2 wt.%), accompanied by lower FeO contents (29–32 wt.%) and elevated TiO_2 contents (54–57 wt.%) (Fig. 10). These analyses showed a lower total than the low-Mn ilmenites (Suppl. Data), which may be explained by a higher amount of trace elements (Kaminsky and Belousova 2009) such as Co, Nb, V, and Zr. The content of V in ilmenite ranges from 54 to 911 ppm, Zr from 17 to 646 ppm, and Nb from 15 to 463 ppm (details are given in Suppl. Data). According to the chondrite normalized trace element patterns (Fig. 7C), the low-Mn ilmenites show an

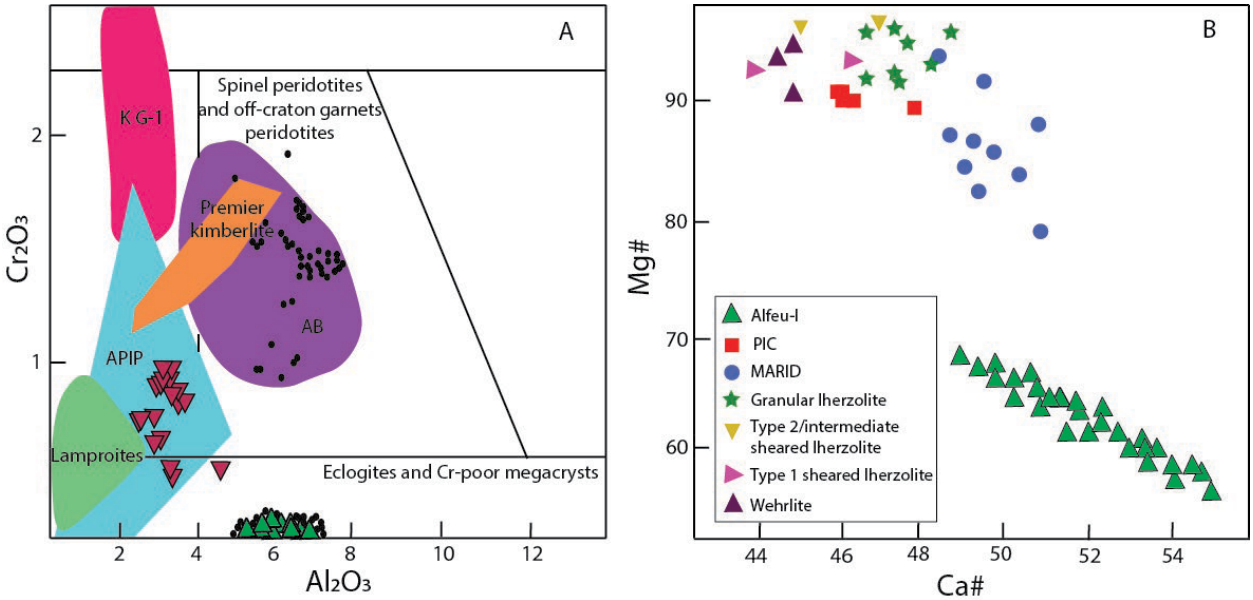

Figure 5. (A) Cr_2O_3 versus Al_2O_3 (wt.%) (modified after Nimis 1998, Barabino *et al.* 2007) and (B) Mg# ((100*Mg)/(Mg+Fe)) versus Ca# ((100*Ca)/(Ca+Mg)) (modified after Fitzpayne *et al.* 2019 and 2020) with Alfeu-I clinopyroxenes plotted as green triangles and orthopyroxenes as purple triangles. For comparison, in (A): black circles are high- and low-Cr clinopyroxenes from Lages diatremes (Barabino *et al.* 2007); KG-1: clinopyroxenes from kimberlites of Gibeon Province (Namibia) (Franz *et al.* 1996, Davies *et al.* 2001); Premier kimberlites field from Kaapvaal Craton, South Africa (Grégoire *et al.* 2005); AB clinopyroxenes from spinel; spinel+garnet and garnet-peridotites from alkali basalt-like magmas after Princivalle *et al.* (1989, 2000), Ionov *et al.* (1993), and Kempton *et al.* (1999); APIP: peridotite nodules from pipes of the Alto Paranaíba Province (Meyer and Svisero 1991, Meyer *et al.* 1991, Araújo *et al.* 2001) and Lamproites field from Mitchell and Bergman (1991). For comparison, in diagram (B): PIC (Phlogopite-Ilmenite-Clinopyroxene rocks) and MARID (Mica-Amphibole-Rutile-Ilmenite-Diopside rocks) (Fitzpayne *et al.* 2019 and 2020).

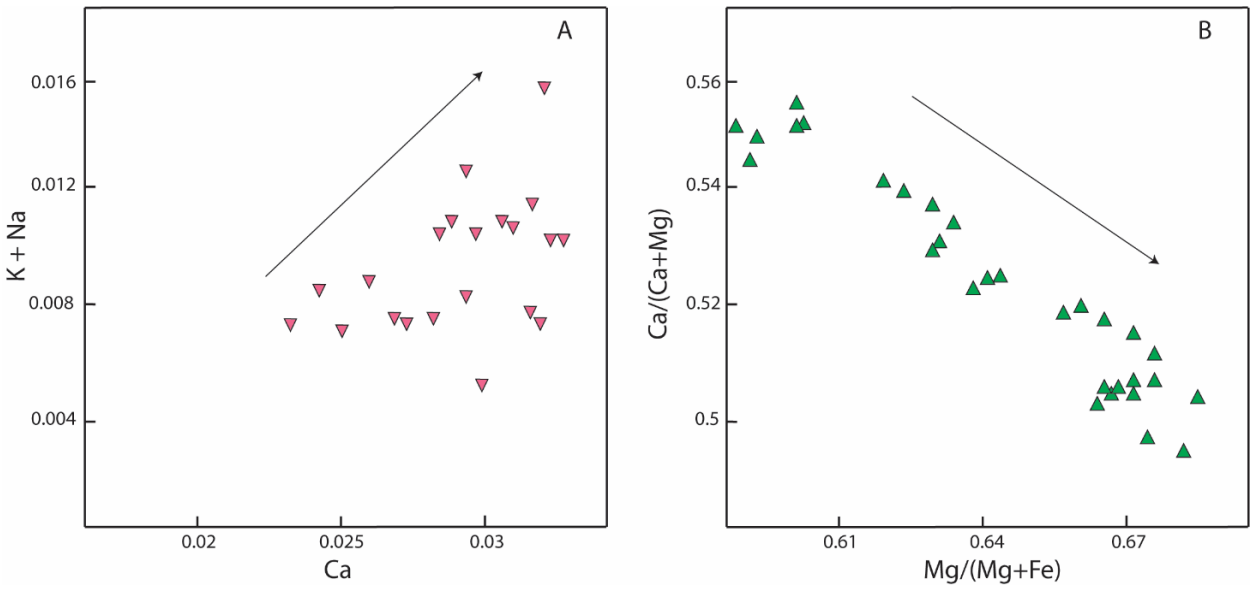

Figure 6. (A) (K+Na) versus Ca (molar) for Alfeu-I orthopyroxenes (inverted pink triangles); (B) Ca/(Ca+Mg) versus Mg/(Mg+Fe) (molar) for Alfeu-I clinopyroxenes (green triangles).

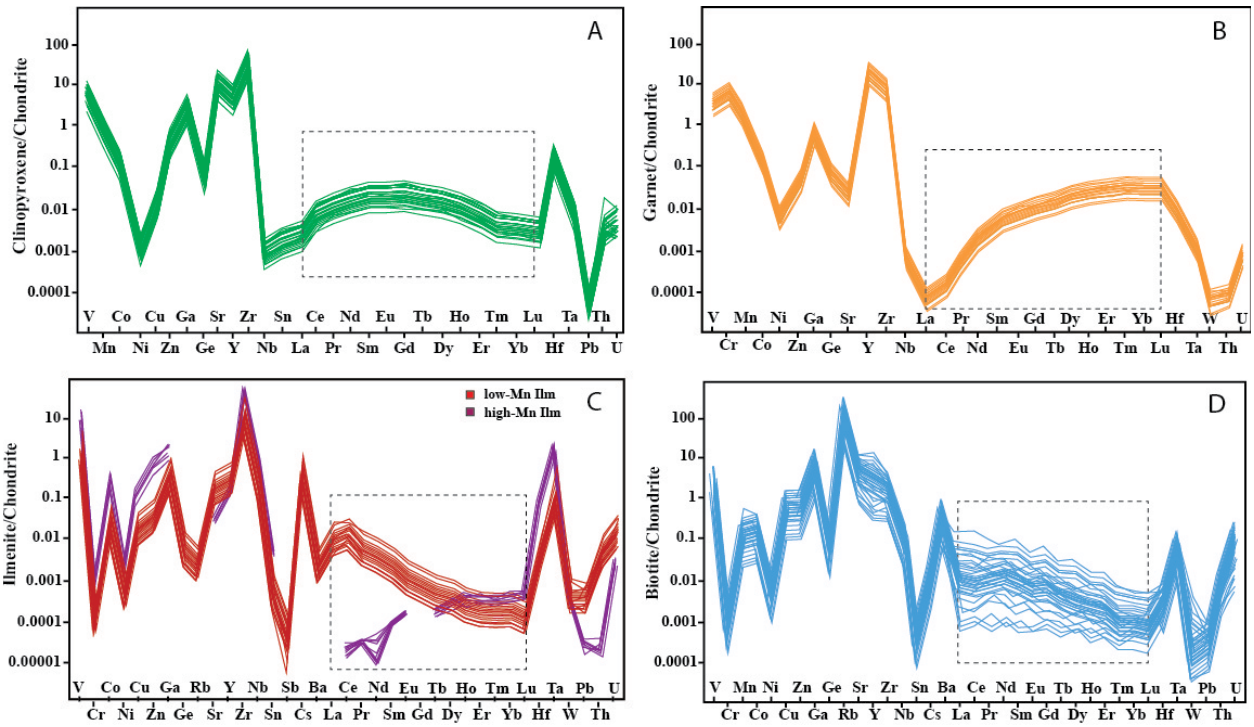

Figure 7. Chondrite normalized (McDonough and Sun 1995) trace element patterns of (A) Alfeu-I clinopyroxene, (B) garnet, (C) ilmenite, and (D) biotite. REE patterns are marked in the dotted squares.

enrichment in LREE relative to HREE, whereas the high-Mn ilmenites show the opposite pattern, which may indicate a depleted source. Both ilmenite groups show positive anomalies of V, Zr, Nb, and Ta.

Mica

Alfeu-I mica macrocrysts and microcrysts have an average composition $(Ca_{0.007}\ Na_{0.25}\ K_{1.8})_{2.06}\ (Ti_{0.9}\ Al_{0.01}\ Fe_{1.92}\ Mn_{0.008}\ Mg_{2.38})_{5.23}\ (Al_{2.37}\ Si_{5.64})_{8.01}\ O_{10}\ (F,OH)_{4.7}$ on the basis of 22 oxygens, were classified as tri-octahedral biotite, following the ternary system Al-Mg-Fe_T (Mitchell 1995) (Fig. 11), and have SiO_2 contents of 35–40 wt.%, MgO of 8.8–12 wt.%, K_2O of 8.7–9.6 wt.%, Al_2O_3 of 12–14 wt.%, and FeO of 12–17 wt.% (details are given in Suppl. Data). In the diagram of the end-member phlogopite $KMg_3AlSi_3O_{10}(OH)_2$ and annite $KFe_3AlSi_3O_{10}(OH)_2$, the composition of Alfeu-I mica is rather different from the groundmass and microphenocryst phlogopites from the Rosário-6 alnöite (Conceição *et al.* 2019). Moreover, we compare our data to phlogopites from Alto Paranaíba kimberlites and kamafugites, Arkhangelsk kimberlite province, calciocarbonatites of Mela Field, Jacupiranga complex carbonatites, and Canadian and Russian kimberlites and carbonatites (Fig. 11).

The cation exchange in the structure of the tri-octahedral biotite with increasing Fe and decreasing Mg and K contents is shown in Fig. 12. The analyzed grains have a content of 294–839 ppm for Mn, 170–459 ppm for Zn, 322–797 for Rb, and 565–1611 ppm for Ba (details are given in Suppl. Data) and have positive anomalies of Rb, Sr, Ba, Zr, Nb, and Ta, as well as an enrichment in LREE (La, Ce, Pr, Nd, Sm, and Eu) compared to HREE (Gd, Tb, Dy, Ho, Er, Tm, Yb, and Lu) (Fig. 7D).

Olivine

Olivine microcrysts ($(Fe_{0.2}Mg_{1.78}Mn_{0.002})_{1.98}SiO_6$ on basis of 4 oxygens) from the Alfeu-I lamproite are rare, with a homogeneous composition of Fo_{89-90} (Suppl. Data). The analyzed minerals have FeO contents of 9.4–9.6 wt.%, MgO of 48–49 wt.%, MnO of 0.13–0.16 wt.%, and NiO of 0.36–0.4 wt.%.

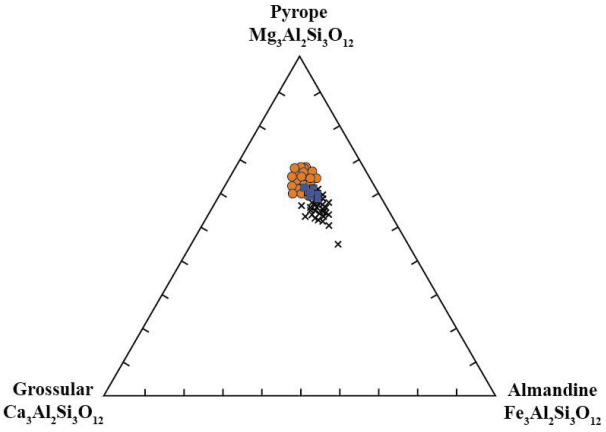

Figure 8. Garnet classification ternary: $Mg_3Al_2Si_3O_{12}$ versus $Fe_3Al_2Si_3O_{12}$ versus $Ca_3Al_2Si_3O_{12}$ with Alfeu-I garnets plotted as orange circles. For comparison, crosses are garnets from Janjão, Pandolfo, and Lambedor diatremes (Brazil) (Barabino *et al.* 2007), and blue squares are from Arkhangelsk Region (Russia) (Shchukina *et al.* 2019).

Sr-Nd isotope data

We performed Rb-Sr and Sm-Nd isotopic analyses of biotite, ilmenite, garnet, and clinopyroxene macrocrysts from Alfeu-I lamproite (Tables 1 and 2), which are used to constrain the Alfeu-I mantle source composition. However, the data from biotite and ilmenite did not result in meaningful data, which indicates the possibility of an open system (Workman and Hart 2005). The $^{87}Rb/^{86}Sr$ ratio was calculated from the elemental concentrations of Rb and Sr. Isotopic data for pyroxene and garnet microcrysts are plotted in Fig. 13A, where we consider the age of 128 Ma obtained via U-Pb in groundmass perovskite from the Rosário 6 alnöite, also found in southern Brazil (Conceição *et al.* 2019), to calculate the $^{87}Sr/^{86}Sr$ and $^{143}Nd/^{144}Nd$ initial ratios for Alfeu-I minerals. The Rosário-6 alnöite age of 128 ± 8 Ma was chosen because it is one of the few alkaline rocks in the area, and its age agrees well with the age of the Paraná flood basalts, which leads us to infer that Alfeu-I lamproite is probably related to both the Rosário-6 and Paraná basalts. We compared these data with the MORB end-member, DMM, HIMU, and EM major mantle reservoirs, and worldwide rocks (Proto Tristan da Cunha plume, Rosário-6 alnöite, Namibia lamprophyres and carbonatites, Alto Paranaíba Igneous Province, Jacupiranga alkaline rocks, sodic and potassic rocks from Paraguay, Patagonian xenoliths, high- and low-Ti Paraná basalts, and Siberian meimechites). Alfeu-I clinopyroxenes plot on the mantle array, within the limits between DMM and EMI reservoirs, close to Rosário-6 alnöite, and within the Proto Tristan da Cunha plume field, whereas garnet has a lower $^{87}Sr/^{86}Sr$ radiogenic ratio but also a lower $^{143}Nd/^{144}Nd$ radiogenic ratio. Based on trace elements patterns (Fig. 7), we suggest that clinopyroxene and garnet were equilibrated with the melt, because both minerals have similar partition coefficients for a range of elements as most REE, Sr, and Y (Harte and Kirkley 1997). If garnet and clinopyroxene crystallized from the same magma at a given time,

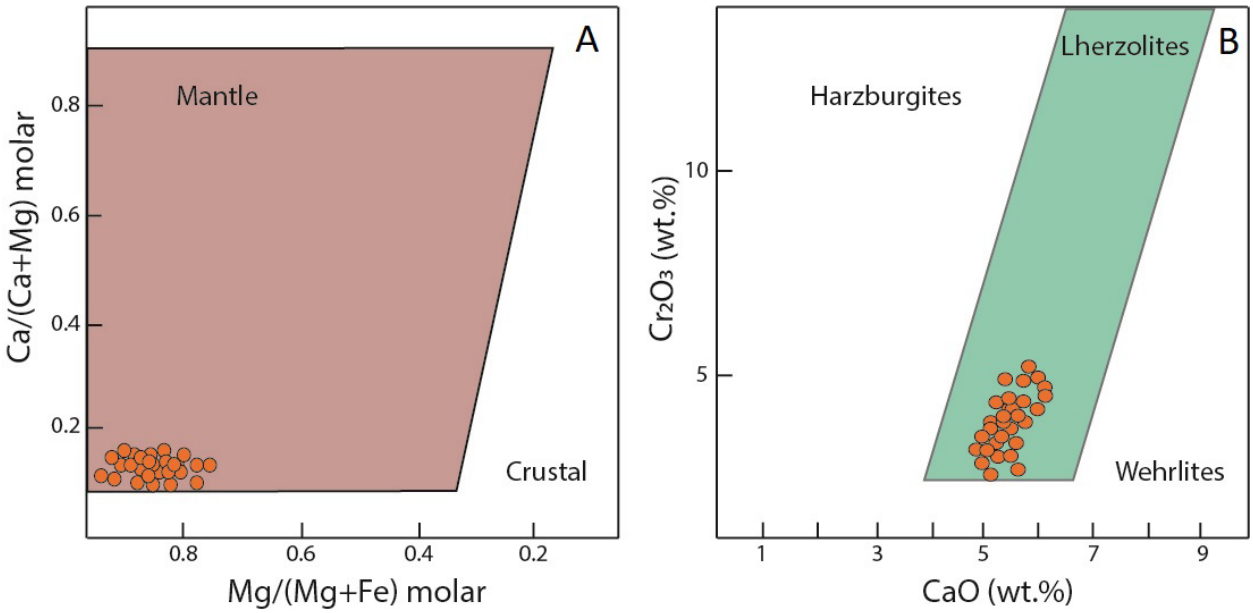

Figure 9. Garnet composition Ca/(Ca+Mg) versus Mg/(Mg+Fe) molar and Cr_2O_3 versus CaO (wt.%) for Alfeu-I (modified from Schulze 2003). The fields in (A) distinguish mantle-derived garnet from those from crustal rocks, and in (B) compositions of garnets from harzburgites, lherzolites, and wehrlites.

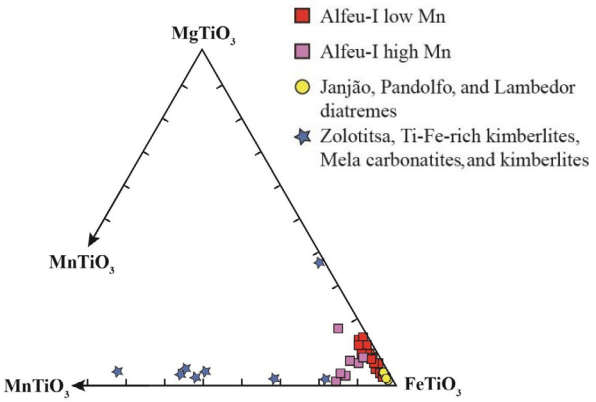

Figure 10. Compositions (mol%) of Alfeu-I ilmenites plotted in the ternary system geikielite ($MgTiO_3$) – ilmenite ($FeTiO_3$) – pyrophanite ($MnTiO_3$) (Mitchell 1995): red squares are from ilmenites with low Mn contents, whereas purple squares are ilmenites with high Mn contents. For comparison, ilmenites from Janjão, Pandolfo, and Lambedor diatremes (Brazil) (Barabino *et al.* 2007) and from diamondiferous Zolotitsa field, Ti-Fe-rich kimberlites, Mela carbonatites, and kimberlites (Arkhangelsk Region, NW Russia) (Beard *et al.* 2000).

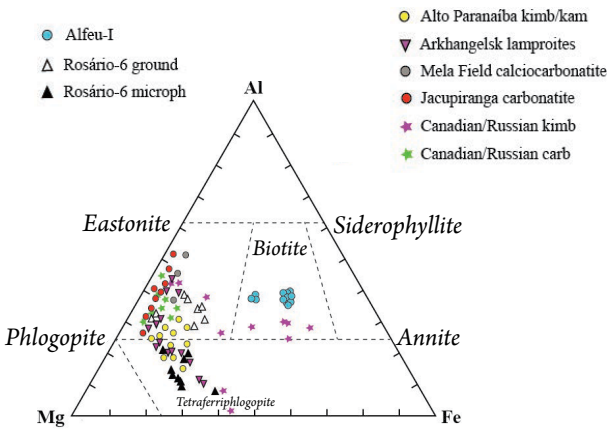

Figure 11. Compositions (22 oxygens) of micas from Alfeu-I lamproite plotted in the ternary diagram Al-Mg-Fe_T, modified after Mitchell (1995). Phlogopite of Rosário-6 alnöite groundmass (white triangles) and microphenocrysts (black triangles) (Conceição *et al.* 2019); Alto Paranaíba kimberlites and kamafugites (yellow circles) (Melluso *et al.* 2008); Arkhangelsk kimberlite province (purple triangles); calciocarbonatite of Mela Field (gray circles) (Beard *et al.* 2000); Jacupiranga carbonatite complex (red circles) (Brod *et al.* 2001); and Canadian and Russian kimberlites and carbonatites (purple and green stars, respectively) (Reguir *et al.* 2009).

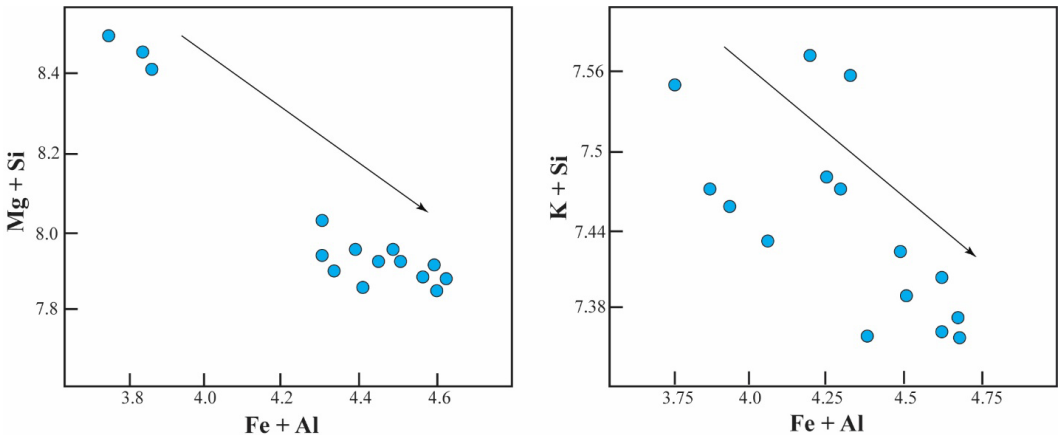

Figure 12. Mg+Si versus Fe+Al and K+Si versus Fe+Al showing the cation exchange in the structure of the tri-octahedral biotite of Alfeu-I lamproite.

Table 1. Rb-Sr isotopic and concentration data obtained through ID-TIMS for pyroxene, garnet, ilmenite, and biotite mineral separates from the Alfeu-I lamproite.

Sample	Mineral	Rb (ppm)	Sr (ppm)	Rb/Sr	$^{87}Rb/^{86}Sr$	Error (abs)	$^{87}Sr/^{86}Sr$	Error (abs)
AF-02-F	Biotite	1167.3806	62.0040	18.8274	54.9073	7.0224	0.7188	0.000093
AF-03-I	Ilmenite	6.6838	4.0622	1.6453	4.8552	0.8914	0.7186	0.000065
AF-04-I	Ilmenite	6.6279	3.9925	1.6600	4.8975	0.9811	0.7186	0.000273
AF-07-P	Pyroxene	1.7830	94.1018	0.0189	0.0552	0.0023	0.7038	0.000219
AF-08-P	Pyroxene	1.4970	92.8910	0.0161	0.0469	0.0018	0.7038	0.000069
AF-05-G	Garnet	6.6426	3.1623	2.1005	6.1663	0.2407	0.7146	0.000271

Table 2. Sm-Nd isotopic and concentration data obtained through ID-TIMS for pyroxene and garnet mineral separates from the Alfeu-I lamproite.

Sample	Mineral	Age (Ma)	Sm (ppm)	Nd (ppm)	$^{147}Sm/^{144}Nd$	$^{143}Nd/^{144}Nd$	$^{143}Nd/^{144}Nd$ (t)	Error (ppm)	Eps Nd	T_{DM} 125 Ma
AF-07-P	Pyroxene	128	23.43	108.71	0.130300	0.512950	0.512841	8	7.18	210
AF-08-P	Pyroxene	128	23.36	90.81	0.155497	0.512830	0.512699	11	4.41	585
AF-05-G	Garnet	128	1044.94	12980.88	0.048669	0.511845	0.511804	16	-13.06	1105

they should display similar initial $^{87}Sr/^{86}Sr$ ratios (Nowell *et al.* 2004, Blackburn *et al.* 2008). Radiogenic ingrowth from ^{87}Rb decay through time in each phase will modify the $^{87}Sr/^{86}Sr$ proportionally, leading to a linear correlation on a $^{87}Sr/^{86}Sr$ versus $^{87}Rb/^{86}Sr$ plot that has a slope proportional to the crystallization age. To perform isochron linear regressions and age calculation, we employed Isoplot/Ex Version 3.75 (Ludwig 2012), which in turn uses the algorithm of York (1969) and error propagation via the maximum-likelihood estimation algorithm of Titterington and Halliday (1979). Albeit three-point isochrons are of doubtful reliability (Ludwig 2012), the crystallization age for the Alfeu-I lamproite magma is 125 ± 11 Ma (Fig. 13B), which closely matches the age of 128±8 Ma obtained with U-Pb dating of perovskite from the Rosário 6 alnöite (Conceição *et al.* 2019).

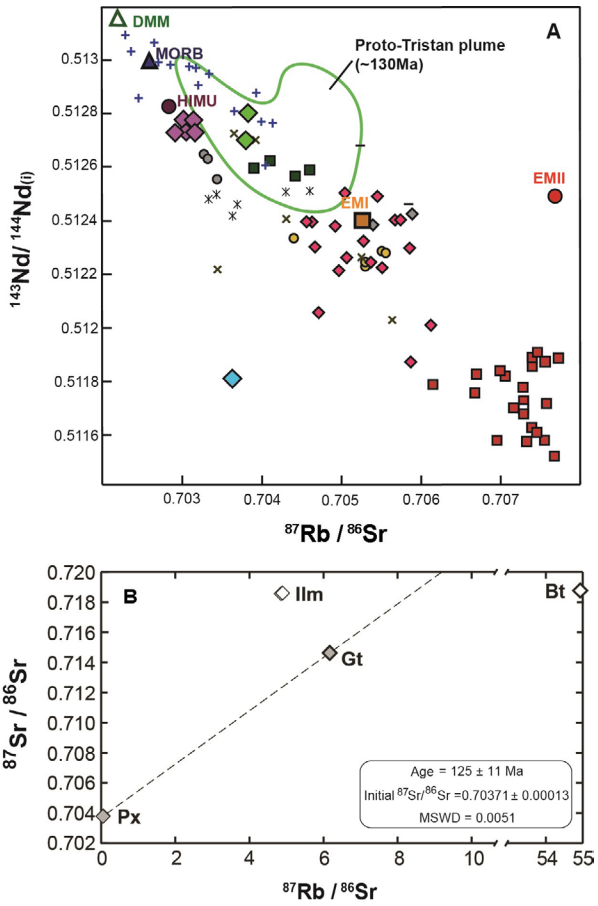

Px: pyroxene; Grt: garnet; Ilm: ilmenite; Bt: biotite.

Figure 13. (A) Sr and Nd isotopic data for pyroxene (green diamonds) and garnet (blue diamond) from the Alfeu-I lamproite. Averages of mantle reservoirs from Hart *et al.* (1992): DMM (Depleted MORB Mantle: open green triangle), MORB (Mid-Ocean Ridge Basalt: blue triangle), HIMU (High-μ: purple circle), EM I (Enriched Mantle I: orange square), and EM II (Enriched Mantle II: red circle). For comparison, the field of Proto Tristan da Cunha plume (~130 Ma Paraná-Etendeka magmas) (Cohen and O'Nions 1982, Gibson *et al.* 1999), Rosário-6 alnöite bulk rock (purple diamonds) (Conceição *et al.* 2019), Namibia lamprophyres and carbonatites (green squares and stars, respectively) (Le Roex and Lanyon 1998), Alto Paranaíba Igneous Province (yellow circles) (Guarino *et al.* 2013), Jacupiranga alkaline rocks (pink diamonds) (Chmyz *et al.* 2017), sodic and potassic rocks from Paraguay ("x" symbols and red squares, respectively) (Comin-Chiaramonti *et al.* 1997), and Patagonian xenoliths (blue crosses) (Jalowitzki *et al.* 2017) are calculated to 128 Ma, while high- and low-Ti Paraná basalts (gray diamonds and traces, respectively) (Marques *et al.* 1999) are calculated to 133 Ma and Siberian meimechites are calculated to 245 Ma (gray circles) (Arndt *et al.* 1995). (B) Rb-Sr mineral isochron for mineral separates (pyroxene, garnet, ilmenite, and biotite) from the Alfeu-I lamproite. Uncertainties are 1σ of the mean value and given in Table 1. Isochron regressions considering both biotite and ilmenite (white diamonds) did not yield meaningful results (see text for details).

Geothermobarometry and oxygen barometry results

Crystallization temperatures of Alfeu-I lamproite were determined using the olivine-spinel Mg-Fe^{2+} exchange geothermometer of O'Neill and Wall (1987) and Ballhaus *et al.* (1991), who applied their geothermometer to peridotite xenoliths. We used chromites and olivines microcrysts analyses of Alfeu-I lamproite (Chaves *et al.* 2014, Provenzano 2016; and this study – Table 3 and Suppl. data) from mineral separates, as the Alfeu-I pipe is unfortunately very altered and it was not possible to collect preserved samples. The Fe^{2+} and Fe^{3+} contents of chromites were calculated with the method of Droop (1987), based on stoichiometric criteria and assuming that all Fe is the only multivalent element and oxygen is the only anion. The calculated mean temperature of Alfeu-I lamproite

Table 3. Alfeu-I equilibrium temperatures and oxygen fugacities calculated based on olivine-chromite geothermometer and the oxygen geobarometer of Ballhaus *et al.* (1991). Olivine compositions are from this study. Chromite compositions from Chaves *et al.* (2014). Olivines (Ol), chromites (Chr), ΔFMQ (fO_2 relative to FMQ buffer), and standard deviations (stdev) as last significant digits in brackets.

Sample		Ol-sp T (°C)		Ol-sp $\Delta\log(fO_2)^{FMQ}$	
		4 GPa	5 GPa	4 GPa	5 GPa
Ol	01	1,489	1,509	2.2	2.0
Chr	Alf-Cr-01				
Ol	02	1,404	1,420	2.8	2.6
Chr	Alf-Cr-02				
Ol	03	1,281	1,301	2.4	2.1
Chr	Alf-Cr-04				
Ol	04	1,322	1,341	2.4	2.1
Chr	Alf-Cr-05				
Ol	05	1,314	1,333	2.3	2.1
Chr	Alf-Cr-06				
Ol	06	1,343	1,362	2.3	2.1
Chr	Alf-Cr-07				
Ol	07	1,623	1,433	2.5	2.4
Chr	Alf-Cr-08				
Ol	08	1,415	1,439	2.3	2.1
Chr	Alf-Cr-11				
Ol	09	1,393	1,412	2.3	2.1
Chr	Alf-Cr-12				
Mean		1,375	1,395	2.4	2.2
(stdev)		(65)	(65)		

crystallization is 1,375(± 65)°C at 4 GPa and 1,395(± 65)°C at 5 GPa (Table 3). To constrain the depth at which the Alfeu-I lamproite melt crystallized, we used the mineral assembly, which suggests a crystallization pressure higher than the crystallization pressure of Rosário-6 alnöite (Carniel *et al*. 2020). This depth range was confirmed by garnet-orthopyroxene geothermobarometry (Nickel and Green 1985). The monticellite in Rosário-6 assembly indicates that the pressure limit for its mantle source is around 3 GPa, whereas the presence of garnet in Alfeu-I assembly suggests a higher source depth. If we compare the results of Alfeu-I lamproite and Rosário-6 alnöite, we can conclude that Alfeu-I crystallization conditions are very similar to those of Rosário-6 alnöite, which gave us more confidence in the use of mineral separates for this geothermobarometry and also suggests that these minerals should be in equilibrium. We also applied the garnet-orthopyroxene geobarometer of Nickel and Green (1985) to Alfeu-I minerals. Calculated Alfeu-I pressure, using temperatures between 1,375 and 1,395°C (Ballhaus *et al*. 1991), is 4.0(± 0.2) GPa, which corresponds to a depth of around 120 km.

The oxygen barometer developed by Ballhaus *et al*. (1991) can be applied to a variety of mantle-derived rocks and spinel-bearing primitive melts. However, the equation is valid only if the silica activity (a_{SiO2}) is buffered by the presence of both olivine and orthopyroxene. In this case, the calculated mean of Alfeu-I oxygen fugacity relative to the fayalite-magnetite-quartz buffer (ΔFMQ) for 4 GPa is 2.4, and for 5 GPa it is 2.2 (Table 3).

DISCUSSION

Alfeu-I mantle source constraints based on mineral composition and isotope data

Based on the major and trace elements of Alfeu-I minerals, we can interpret that its mantle source has been metasomatized, which is reflected by the almost flat REE pattern of clinopyroxene, with a slight enrichment of MREE relative to LREE and HREE (McDonough and Frey 1989) (Fig. 7A). The Alfeu-I pyroxenes suggest two distinct genetic episodes, as the clinopyroxenes have an eclogite signature and the orthopyroxenes contain a peridotite signature (Fig. 5A), which is associated with the high Cr content. Figure 5A (Cr_2O_3 versus Al_2O_3 and Cr versus Fe versus Na molar) shows that Alfeu-I clinopyroxenes plot in the eclogites and Cr-poor megacrysts fields, which indicates that their mantle source may have been metasomatized by fluids derived from a subducted slab (Shu *et al*. 2018, Skuzovatov *et al*. 2022). The chondrite-normalized garnet and clinopyroxene trace element patterns are similar (Figs. 7A and 7B), which may suggest that both minerals were equilibrated in the melt (Harte and Kirkley 1997). The Alfeu-I pyropes have a depleted mantle signature, evidenced by the enrichment in HREE relative to LREE, and this reflects the incompatible element-depleted nature of the upper mantle from which these magmas are derived or passed by (Klein-BenDavid and Pearson 2009). The positive anomalies of Rb, Sr, Ba, Zr, Nb, and Ta in high-Mn ilmenites and the enrichment of LREE relative to HREE of low-Mn ilmenites occur due to structural reasons. However, it may also indicate a metasomatic process that may be caused by slab contamination of the mantle. The slabs may have been partially melted at high temperature and pressure, releasing HFS elements and causing the positive anomalies of, for example, Nb and Ta.

These metasomatic processes in the depleted mantle may have been caused by fluids from recycled oceanic crust, low degree melts in the upper mantle that act as enriching agents for the peridotite source region, or the presence of detached sub-continental lithospheric mantle that remained in the asthenosphere after the breakup (Hawkesworth *et al*. 1986, Peate *et al*. 1999). The Gondwana breakup probably initiated in the mid-Jurassic; however, the exact timing is uncertain, considering that the oldest magnetic anomalies on the South Atlantic oceanic crust have associated ages from 135 and 126 Ma (Nürnberg and Müller 1991, Turner *et al*. 1994, Hall *et al*. 2018). The Paraná flood basalts are one of the most important events that occurred during the continental separation, and they provide significant information about the sub-continental mantle in this region. These basalts are divided into low- and high-Ti groups, the latter with higher Fe, P, Ti, Zr, Ce, La, Ba, and Sr concentrations (Bellieni *et al*. 1984). This compositional variation is interpreted by the authors as evidence of a large-scale heterogeneous mantle source beneath this region during the breakup. In addition to previous studies (Marques *et al*. 1999, Peate *et al*. 1999) that proposed heterogeneous lithospheric mantle melting as the source of the Paraná flood basalts, Rocha-Júnior *et al*. (2012, 2013) demonstrated, based on Re-Os and Sr-Nd-Pb isotopic data, that the asthenospheric source of the basalts was enriched by fluids or magmas related to the Neoproterozoic subduction processes. The authors also suggested that the Tristan da Cunha mantle plume could have acted as a heat source that may have triggered the generation of the Paraná flood basalts (Jennings *et al*. 2019). According to a number of authors (Comin-Chiaramonti *et al*. 1997, 2002, Gibson *et al*. 1995, 2006, Marques *et al*. 2016), extensional tectonic movements caused by the Gondwana breakup triggered the basaltic lava eruption that covered the Paraná basin sediments. These movements may also have been responsible for smaller alkaline events such as the Rosário-6 alnöite (Conceição *et al*. 2019, Carniel *et al*. 2020) and the Alfeu-I lamproite in greater depths.

As clinopyroxene prefers to incorporate Sr over Rb (Beattie 1993, Foley *et al*. 1996, Leitzke *et al*. 2017), the low Rb/Sr ratio of clinopyroxene will constraint the initial $^{87}Sr/^{86}Sr$ for the kimberlite and other-alkaline related magmas (Blackburn *et al*. 2008). Pyroxenes plot between DMM and EMI plots, close to Rosário-6 alnöite and inside the Proto Tristan da Cunha plume field, whereas garnet has a lower $^{87}Sr/^{86}Sr$ and $^{143}Nd/^{144}Nd$ radiogenic ratio. The values for Sr isotopes acquired in biotite are high, indicating upper continental crust origin. It is likely that clinopyroxene reflects the source of the kimberlite, while biotite was generated in a shallower, crustal environment due to metasomatic processes. The crystallization age suggested in this study (125 Ma) also indicates a possible correlation between Alfeu-I lamproite and Rosário-6 alnöite (128 Ma) events.

Alfeu-I lamproite tectonic settings

The fO_2 conditions during Paraná flood basalt genesis are representative of the mantle redox conditions in this region during the beginning of the continental breakup. As the most expressive event that occurred during the Gondwana breakup in southern Brazil, its redox conditions may contribute to evaluating how oxidized the Alfeu-I lamproite is compared to this mantle source. The fO_2 conditions calculated for the Alfeu-I lamproite and Rosário-6 alnöite are significantly higher than the fO_2 of the Paraná flood basalts, as described by Bellieni *et al.* (1984) (Fig. 14). The latter authors used the method of Buddington and Lindsley (1964) to determine the fO_2 of the Serra Geral basalts based on ilmenite and Ti-magnetite compositions. They found that high-Ti basalts, which have fO_2 values between the nickel-nickel oxide (NNO) and fayalite-magnetite-quartz (FMQ) buffers, are slightly more oxidized than the low-Ti basalts, with fO_2 values between the FMQ and wüstite-magnetite (WM) buffers, which can be correlated to the Ti-enrichment and the source depth of these rocks. High-Ti basalts have been derived from greater depths (90–120 km depth), with a lower degree of melting than the low-Ti basalts (30–60 km depth) (Garland *et al.* 1996).

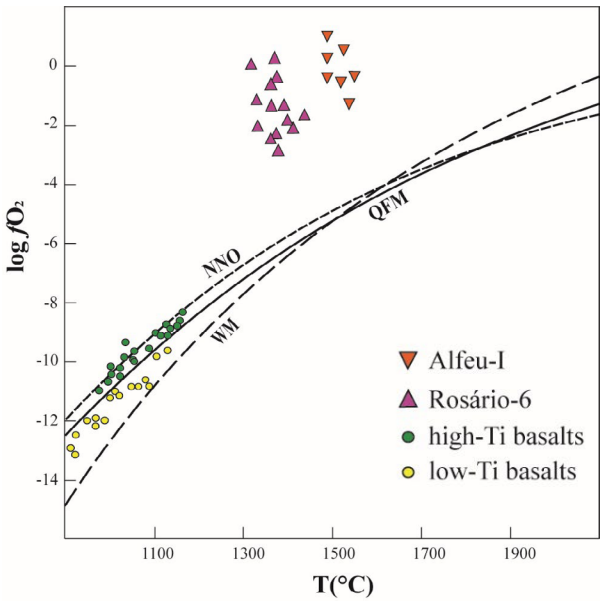

Figure 14. LogfO_2 versus temperature with calculated T and fO_2 for Alfeu-I lamproite (inverted orange triangles); Rosário-6 (purple triangles); high-Ti Serra Geral basalts (green circles); and low-Ti Serra Geral basalts (yellow circles) (Bellieni *et al.* 1984) results. Buffers: NNO (nickel-nickel oxide); FMQ (fayalite-magnetite-quartz) (Ballhaus *et al.* 1991); and WM (wüstite-magnetite) (O'Neill 1988).

Recent studies (Conceição *et al.* 2019, Carniel *et al.* 2020) on the mantle source of alkaline rocks in southern Brazil show a close link between these occurrences and the Gondwana continental breakup and the opening South Atlantic, which started at ca. 135 Ma ago (Hall *et al.* 2018). Following these authors, subducting slabs that contained carbonated sediments and metabasalts could be responsible for metasomatic processes in the mantle, which may have been oxidized and chemically enriched by carbonatite and/or silicate melt metasomatism (Fumagalli and Klemme 2015, Gervasoni *et al.* 2017). The origin of these hydrated and carbonated fluids or melts that caused such a melt oxidation process in Alfeu-I lamproite may be related to subducting materials from old subduction processes similar to the Rosário-6 alnöite (Conceição *et al.* 2019).

Based on our calculations, Alfeu-I lamproite may have crystallized at a pressure of 4–5 GPa, which corresponds to around 120–150 km depth, temperatures between 1,375 and 1,395°C, and at $\Delta FMQ = 2.4–2.2$. Alfeu-I temperatures and fO_2 are plotted in the diagram (Fig. 15), where D/GCO is the diamond/graphite-carbon oxide buffer from Frost and Wood (1997), EMOD/G is the enstatite-magnesite-olivine-diamond/graphite buffer from Zhao *et al.* (1999), and NNO is the nickel-nickel oxide buffer from Ballhaus *et al.* (1991). The GCO and DCO oxygen buffers describe the upper fO_2 stability of

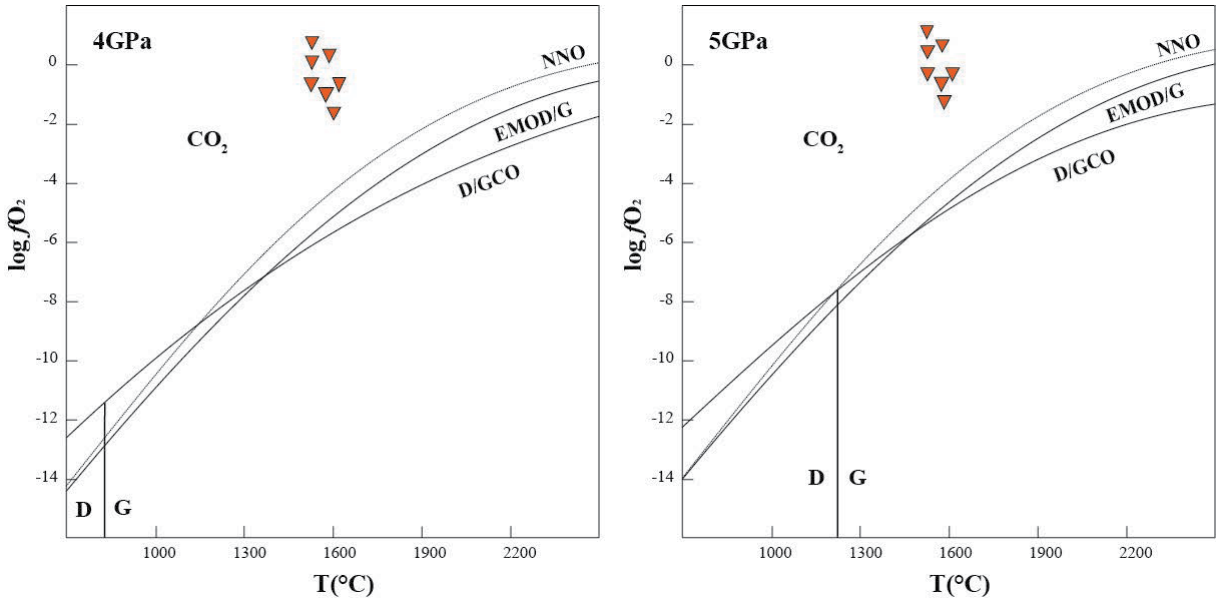

Figure 15. Stability fields of graphite and CO_2 in logfO_2 versus temperature diagram at 4 and 5 GPa. D/GCO buffer from Frost and Wood (1997); EMOD/G buffer from Zhao *et al.* (1999); and NNO buffer from Ballhaus *et al.* (1991). The D/G (diamond/graphite) limit is from Kennedy and Kennedy (1976). Alfeu-I results are plotted as inverted orange triangles.

graphite or diamond with respect to a free C-O fluid (Frost and Wood 1997). The EMOD/G curve defines the stability field between diamond/graphite and magnesite ($MgCO_3$) in the mantle. Considering this, the area below this curve represents the oxygen fugacity for melts in equilibrium with diamond or graphite, and the Alfeu-I oxygen fugacity plots above the graphite stability curve (Fig. 15). At such conditions, carbon can be oxidized to produce carbonate melt through the reduction of Fe^{3+} in silicate minerals during upwelling (Rohrbach and Schmidt 2011, Stagno *et al*. 2013). From 4 to 5 GPa (120–150 km depth), diamonds can be stable only at very low oxygen fugacities and at low temperatures (see D/G limit in Fig. 15).

CONCLUSION

We present new mineralogical and geochemical data on the Alfeu-I lamproite. It exhibits an inequigranular texture with macrocrysts of mica, chromite, garnet, and ilmenite and microcrysts of mica, pyroxene, and rare olivine, all immersed in a groundmass composed of pyroxene, chromite, perovskite, rutile, ilmenite, and, more rarely, olivine. Major and trace elements of Alfeu-I minerals indicate a depleted mantle source that was re-fertilized by metasomatic processes in the lithosphere. The Sr-Nd isotopic data and the Rb-Sr isochron, based on the pyroxene and garnet isotope compositions, indicate a metasomatized mantle source and crystallization age close to Rosário-6 alnöite. An enriched mantle source is considered to have been the product, for example, of metasomatism acting on the subcontinental lithospheric mantle after subduction ceases, which would lead to the formation of alkali-enriched magmas that can have a mantle signature. Therefore, we consider that the negative εNd values imply an enriched mantle source, i.e., a mantle that was metasomatized by fluids in a previous subduction setting (Zi *et al*. 2012). Garnet and clinopyroxene could come from two distinct sources, which would not be surprising given that this rock occurs in diatremes and the mantle beneath Gondwana during the breakup was not homogeneous. The Alfeu-I lamproite may have crystallized at pressures between 4 and 5 GPa, which corresponds to around 120–50 km depth, at high temperatures (from 1,375 to 1,395°C) and relatively oxidized conditions, at ΔFMQ = +2.4 to +2.2. The origin of the metasomatic agents that caused such a melt oxidation process in Alfeu-I lamproite may be related to subducted slab materials from old subduction processes in the mantle source.

ACKNOWLEDGMENTS

This research was supported by Conselho Nacional de Desenvolvimento Científico e Tecnológico – Brazil (CNPq – 141241/2013-6), Fundação de Amparo à Pesquisa do Estado do Rio Grande do Sul – Brazil (FAPERGS – Edital 05/2019), and the project "Diamante Brasil" from the Geological Survey of Brazil (CPRM). We are very grateful to Prof. Márcia E. B. Gomes, Susan Drago, MSc, and Daniel Grings Cedeño, MSc, for their help with Alfeu-I microprobe data acquisition, and to Beate Schmitt for her assistance with LA-ICP-MS data. We also thank João Wustrow, who separated the Alfeu-I minerals, and Mariana da Silva Assis, MSc, for her help with the isotope analyses.

ARTICLE INFORMATION

Manuscript ID: 20220092. Received on: 23 NOV 2022. Approved on: 06 JUN 2023.

How to cite: Carniel L.C., Conceição R.V., Provenzano C.A.S., Sander A., Leitzke F.P., Silva A.B., Berndt J., Klemme S. (2023). Mineral chemistry from the Alfeu-I lamproite (Southern Brazil) and its contribution to understand the mantle heterogeneity under South American Plate during the Gondwana breakup. *Brazilian Journal of Geology*, **53**(3), e20220092. https://doi.org/10.1590/2317-4889202320220092

L.C.C.: Conceptualization, Data curation, Formal analysis, Funding acquisition, Investigation, Methodology, Visualization, Writing – original draft, Writing – review & editing. R.V.C.: Conceptualization, Data curation, Formal analysis, Funding acquisition, Investigation, Project administration, Supervision, Validation, Writing – review & editing. C.A.S.P.: Conceptualization, Data curation, Formal analysis, Funding acquisition, Investigation. A.S.: Conceptualization, Data curation, Investigation, Supervision, Validation, Writing – review & editing. F.P.L.: Data curation, Formal analysis, Investigation, Methodology, Validation, Visualization, Writing – review & editing. A.B.S.: Investigation, Methodology, Validation, Visualization. J.B.: Data curation, Formal analysis, Methodology, Validation, Writing – review & editing. S.K.: Investigation, Methodology, Supervision, Validation, Writing – review & editing.

Competing interests: the authors declare that there are no competing interests.

REFERENCES

Almeida F.F.M. 1983. Relações tectônicas das rochas alcalinas mesozoicas da região meridional da Plataforma Sul-Americana. *Revista Brasileira de Geociências*, **13**(3):139-158.

Araújo A.L.N., Carlson R.W., Gaspar J.C., Bizzi L.A. 2001. Petrology of kamafugite and kimberlites from the Alto Paranaíba Alkaline Province, Minas Gerais, Brazil. *Contributions to Mineralogy and Petrology*, **142**(2), 163-177. https://doi.org/10.1007/s004100100280

Arndt N., Lehnert K., Vasil'ev Y. 1995. Meimechites: highly magnesian lithosphere contaminated alkaline magmas from deep subcontinental mantle. *Lithos*, **34**(1-3), 41-59. https://doi.org/10.1016/0024-4937(95)90009-8

Ballhaus C., Berry R.F., Green D.H. 1991. High pressure experimental calibration of the olivine-orthopyroxene-spinel oxygen geobarometer: implications for the oxidation state of the upper mantle. *Contributions to Mineralogy and Petrology*, **107**, 27-40. https://doi.org/10.1007/BF00311183

Barabino G., Gomes C.B., Traversa G. 2007. The Lages diatremes: mineral composition and petrological implications. *Anais da Academia Brasileira de Ciências*, **79**(3), 473-501. https://doi.org/10.1590/S0001-37652007000300010

Barbieri M., Beccaluva L., Brotzu P., Conte A., Garbarino C., Gomes C.B., Loss E., Morbidelli L., Scheibe L.F., Tamura R.M. 1987. Petrological and Geochemical Studies of Alkaline Rocks from Continental Brazil. 1. The phonolite Suite from Piratini, RS. *Geochimica Brasiliensis*, **1**, 109-138.

Beard A.D., Downes H., Hegner E., Sablukov S.M. 2000. Geochemistry and mineralogy of kimberlites from the Arkhangelsk Region, NW Russia: evidence for transitional kimberlite magma types. *Lithos*, **51**(1-2), 47-73. https://doi.org/10.1016/S0024-4937(99)00074-2

Beattie P. 1993. The effect of partial melting of spinel peridotite on uranium series disequilibria: constraints from partitioning studies. *Earth and Planetary Science Letters*, **177**(3-4), 379-391. https://doi.org/10.1016/0012-821X(93)90091-M

Bellieni G., Comin-Chiaramonti P., Marques L.S., Melfi A.J., Piccirillo E.M., Nardy A.J.R., Roisenberg A. 1984. High- and low- TiO_2 flood basalts from the Paraná plateau (Brazil): petrology and geochemical aspects bearing on their mantle origin. *Neues Jahrbuch für Mineralogie*, **150**(3), 273-306.

Beyer C., Berndt J., Tappe S., Klemme S. 2013. Trace element partitioning between perovskite and kimberlite to carbonatite melt: New experimental constraints. *Chemical Geology*, **353**, 132-139. https://doi.org/10.1016/j.chemgeo.2012.03.025

Blackburn T.J., Stockli D.F., Carlson R.W., Berendsen P. 2008. (U–Th)/He dating of kimberlites—A case study from north-eastern Kansas. *Earth and Planetary Science Letters*, **275**(1-2), 111-120. https://doi.org/10.1016/j.epsl.2008.08.006

Brod J.A., Gaspar J.C., de Araújo D.P., Gibson S.A., Thompson R.N., Junqueira-Brod T.C. 2001. Phlogopite and tetra-ferriphlogopite from Brazilian carbonatite complexes: petrogenetic constraints and implications for mineral-chemistry systematics. *Journal of Asian Earth Sciences*, **19**(3), 265-296. https://doi.org/10.1016/S1367-9120(00)00047-X

Buddington A.F., Lindsley D.H. 1964. Iron-Titanium Oxide Minerals and Synthetic Equivalents. *Journal of Petrology*, **5**(2), 310-357. https://doi.org/10.1093/petrology/5.2.310

Carniel L.C., Conceição R.V., Klemme S., Berndt J., Jalowitzki F. 2020. Origin and redox conditions of the Rosário-6 alnöite of southern Brazil: implications for the state of the mantle during Gondwana breakup. *Lithos*, **376-377**, 105751. https://doi.org/10.1016/j.lithos.2020.105751

Chaves M.L.S.C., Andrade K.W., Azzi A.A., Silveira F.V. 2014. Minerais indicadores kimberlíticos e prospectividade diamantífera da intrusão Alfeu-01 (Canguçu, RS). *Geociências*, **33**(4), 535-548.

Chmyz L., Arnaud N., Biondi J.C., Azzone R.G., Bosch D., Ruberti E. 2017. Ar-Ar ages, Sr-Nd isotope geochemistry, and implications for the origin of the silicate rocks of the Jacupiranga ultramafic-alkaline complex (Brazil). *Journal of South American Earth Sciences*, **77**, 286-309. https://doi.org/10.1016/j.jsames.2017.05.009

Cohen R.S., O'Nions R.K. 1982. Identification of recycled continental material in the mantle from Sr, Nd and Pb isotope investigations. *Earth and Planetary Science Letters*, **61**(1), 73-84. https://doi.org/10.1016/0012-821X(82)90040-1

Comin-Chiaramonti P., Cundari A., Piccirillo E.M., Gomes C.B., Castorina F., Censi P., De Min A., Marzoli A., Speziale S., Velázquez V.F. 1997. Potassic and sodic igneous rocks from Eastern Paraguay: their origin from the lithospheric mantle and genetic relationships with associated Parana flood tholeiites. *Journal of Petrology*, **38**(4), 495-528. https://doi.org/10.1093/petroj/38.4.495

Comin-Chiaramonti P., Gomes C.B., Castorina F., Di Censi P., Antonini P., Furtado S., Ruberti E., Scheibe L.F. 2002. Geochemistry and geodynamic implications of the Anitápolis and Lages alkaline-carbonatite complexes, Santa Catarina State, Brazil. *Revista Brasileira de Geociências*, **32**(1), 43-58.

Conceição R.V., Carniel L.C., Jalowitzki T., Gervasoni F., Cedeño D.G. 2019. Geochemistry and geodynamic implications on the source of Paraná-Etendeka Large Igneous Province evidenced by the 128 Ma Rosário-6 kimberlite, southern Brazil. *Lithos*, **328-329**, 130-145. https://doi.org/10.1016/j.lithos.2019.01.012

Davies G.R., Spriggs A.J., Nixon P.H. 2001. A noncognate origin for the Gibeon kimberlite megacryst suite, Namibia: implications for the origin of Namibian kimberlites. *Journal of Petrology*, **42**(1), 159-172. https://doi.org/10.1093/petrology/42.1.159

Droop G.T.R. 1987. A general equation for estimating Fe^{3+} concentrations in ferromagnesian silicates and oxides from microprobe analyses, using stoichiometric criteria. *Mineralogical Magazine*, **51**(361), 431-435. https://doi.org/10.1180/minmag.1987.051.361.10

Fitzpayne A., Giuliani A., Harris C., Thomassot E., Cheng C., Hergt J. 2019. Evidence for subduction-related signatures in the southern African lithosphere from the N-O isotopic composition of metasomatic mantle minerals. *Geochimica et Cosmochimica Acta*, **266**, 237-257. https://doi.org/10.1016/j.gca.2019.02.037

Fitzpayne A., Giuliani A., Hergt J., Woodhead J.D., Maas R. 2020. Isotopic analyses of clinopyroxenes demonstrate the effects of kimberlite melt metasomatism upon the lithospheric mantle. *Lithos*, **370-371**, 105595. https://doi.org/10.1016/j.lithos.2020.105595

Foley S.F., Jackson S.E., Fryer B.J., Greenough J.D., Jenner G.A. 1996. Trace element partition coefficients for clinopyroxene and phlogopite in an alkaline lamprophyre from Newfoundland by LAM-ICP-MS. *Geochimica et Cosmochimica Acta*, **60**(4), 629-638. https://doi.org/10.1016/0016-7037(95)00422-X

Fragoso-César A.R.S. 1991. *Tectônica de Placas no Ciclo Brasiliano: As orogenias dos Cinturões Dom Feliciano e Ribeira no Rio Grande do Sul*. Ph.D. thesis, University of São Paulo, São Paulo, 367 p.

Franz L., Brey G.P., Okrusch M. 1996. Steady state geotherm, thermal disturbances, and tectonic development of the lower lithosphere underneath the Gibeon Kimberlite Province, Namibia. *Contributions to Mineralogy and Petrology*, **126**, 181-198. https://doi.org/10.1007/s004100050243

Frost D.J., Wood B.J. 1997. Experimental measurements of the fugacity of CO_2 and graphite/diamond stability from 35 to 77 kbar at 925°C to 1650°C. *Geochimica et Cosmochimica Acta*, **61**(8), 1565-1574. https://doi.org/10.1016/S0016-7037(97)00035-5

Fumagalli P., Klemme S. 2015. Mineralogy of the Earth: Phase Transitions and Mineralogy of the Upper Mantle. In: Schubert G. (ed.), *Mineral Physics. Treatise on Geophysics*. Elsevier. v. 2. p. 33-62.

Garland F., Turner S., Hawkesworth C. 1996. Shifts in the source of the Paraná basalts through time. *Lithos*, **37**(2-3), 223-243. https://doi.org/10.1016/0024-4937(95)00038-0

Gervasoni F., Klemme S., Rohrbach A., Grützner T., Berndt J. 2017. Experimental constraints on mantle metasomatism caused by silicate and carbonate melts. *Lithos*, **282-283**, 173-186. https://doi.org/10.1016/j.lithos.2017.03.004

Gibson S.A., Thompson R.N., Day J.A. 2006. Timescales and mechanisms of plume–lithosphere interactions: $^{40}Ar/^{39}Ar$ geochronology and geochemistry of alkaline igneous rocks from the Paraná–Etendeka large igneous province. *Earth and Planetary Science Letters*, **251**(1-2), 1-17. https://doi.org/10.1016/j.epsl.2006.08.004

Gibson S.A., Thompson R.N., Leonardos O.H., Dickin A.P., Mitchell J.G. 1995. The Late Cretaceous Impact of the Trindade Mantle Plume: Evidence from Large-volume, Mafic, Potassic Magmatism in SE Brazil. *Journal of Petrology*, **36**(1), 189-229. https://doi.org/10.1093/petrology/36.1.189

Gibson S.A., Thompson R.N., Leonardos O.H., Dickin A.P., Mitchell J.G. 1999. The limited extent of plume-lithosphere interactions during continental flood-basalt genesis: geochemical evidence from cretaceous magmatism in southern Brazil. *Contributions to Mineralogy and Petrology*, **137**, 147-169. https://doi.org/10.1007/s004100050588

Gomes C.B., Comin-Chiaramonti P. 2017. *Magmatismo alcalino continental da região meridional da Plataforma Brasileira*. São Paulo: Ed. USP, 595 p.

Gomes C.B., Laurenzi M.A., Censi P., De Min A., Velázquez V.F., Comin-Chiaramonti P. 1996. Alkaline magmatism from northern Paraguay (Alto Paraguay): a permo-triassic province. In: Comin-Chiaramonti P., Gomes C.B. (eds.), *Alkaline magmatism in central eastern Paraguay*. Relationships with coeval magmatism in Brazil. São Paulo: Ed. USP, p. 223-230.

Grégoire M., Tinguely C., Bell D.R., Le Roex A.P. 2005. Spinel lherzolite xenoliths from the Premier kimberlite (Kaapvaal craton, South Africa): nature and evolution of the shallow upper mantle beneath the Bushveld complex. *Lithos*, **84**(3-4), 185-205. https://doi.org/10.1016/j.lithos.2005.02.004

Griffin W.L., Powell W.J., Pearson N.J., O'Reilly S.Y. 2008. Glitter: Data reduction software for laser ablation ICP-MS. In: Sylvester P.J. (ed.), *Laser Ablation ICP-MS in the Earth Sciences:* Current Practices and Outstanding Issues, Mineralogical Association of Canada Short Course Series, Short Course 40. Vancouver, p. 308-311.

Guarino V., Wu F., Lustrino M., Melluso L., Brotzu P., Gomes C.B., Ruberti E., Tassinari C.C.G., Svisero D.P. 2013. U–Pb ages, Sr–Nd- isotope geochemistry, and petrogenesis of kimberlites, kamafugites and phlogopite-picrites of the Alto Paranaíba Igneous Province, Brazil. *Chemical Geology*, **353**, 65-82. https://doi.org/10.1016/j.chemgeo.2012.06.016

Hall S.A., Bird D.E., McLean D.J., Towle P.J., Grant J.V., Danque H.A. 2018. New constraints on the age of the opening of the South Atlantic basin. *Marine and Petroleum Geology*, **95**, 50-66. https://doi.org/10.1016/j.marpetgeo.2018.03.010

Hart S.R., Hauri E.H., Oschmann L.A., Whitehead J.A. 1992. Mantle plumes and entrainment: isotopic evidence. *Science*, **256**(5056), 517-520. https://doi.org/10.1126/science.256.5056.517

Harte B., Kirkley M.B. 1997. Partitioning of trace elements between clinopyroxene and garnet: data from mantle eclogites. *Chemical Geology*, **136**(1-2), 1-24. https://doi.org/10.1016/S0009-2541(96)00127-1

Hawkesworth C.J., Mantovani M.S.M., Taylor P.N., Palacz Z. 1986. Evidence from the Parana of South Brazil for a continental contribution to Dupal basalts. *Nature*, **322**, 356-359. https://doi.org/10.1038/322356a0

Ionov D.A., Ashkepkov I.V., Stosh H.G., Witt-Eickschen G.. Seck H.A. 1993. Garnet peridotite from the Vitim Volcanic Field, Baikal region: the nature of the garnet-spinel peridotite transition zone in the continental mantle. *Journal of Petrology*, **34**(6), 1141-1175. https://doi.org/10.1093/petrology/34.6.1141

Jalowitzki T., Gervasoni F., Conceição R.V., Orihashi Y., Bertotto G.W., Sumino H., Schilling M.E., Nagao K., Morata D., Sylvester P. 2017. Slab-derived components in the subcontinental lithospheric mantle beneath Chilean Patagonia: Geochemistry and Sr–Nd–Pb isotopes of mantle xenoliths and host basalt. *Lithos*, **292-293**, 179-197. https://doi.org/10.1016/j.lithos.2017.09.008

Jennings E.S., Gibson S.A., MacLennan J. 2019. Hot primary melts and mantle source for the Paraná-Etendeka flood basalt province: New constraints from Al-in-olivine thermometry. *Chemical Geology*, **529**, 119287. https://doi.org/10.1016/j.chemgeo.2019.119287

Jochum K.P., Nohl L., Herwig K., Lammel E., Toll B., Hofmann A.W. 2005. GeoReM: a new geochemical database for reference materials and isotopic standards. *Geostandards and Geoanalytical Research*, **29**(3), 333-338. https://doi.org/10.1111/j.1751-908X.2005.tb00904.x

Kaminsky F.V., Belousova E.A. 2009. Manganoan ilmenite as kimberlite/diamond indicator mineral. *Russian Geology and Geophysics*, **50**(12), 1212-1220. https://doi.org/10.1016/j.rgg.2009.11.019

Kempton P.D., Hawkeswort C.J., Lopez Escobar L., Pearson D.G., Ware A.J. 1999. Spinel garnet xenoliths from Pali Aike, Part 1: petrography, mineral chemistry and geothermobarometry. In: International Kimberlite Conference, 7 (Dawson Volume). Cape Town, South Africa. *Proceedings*, p. 403-414.

Kennedy C.S., Kennedy G.C. 1976. The Equilibrium Boundary Between Graphite and Diamond. *Journal of Geophysical Research*, **81**(14), 2467-2470. https://doi.org/10.1029/JB081i014p02467

Klein-BenDavid O., Pearson D.G. 2009. Origins of subcalcic garnets and their relation to diamond forming fluids—Case studies from Ekati (NWT-Canada) and Murowa (Zimbabwe). *Geochimica et Cosmochimica Acta*, **73**(3), 837-855. https://doi.org/10.1016/j.gca.2008.04.044

Le Roex A.P., Lanyon R. 1998. Isotope and trace element geochemistry of cretaceous Damaraland lamprophyres and carbonatites, northwestern Namibia: evidence for plume-lithosphere interactions. *Journal of Petrology*, **39**(6), 1117-1146. https://doi.org/10.1093/petroj/39.6.1117

Leitzke F.P., Fonseca R.O.C, Sprung P., Mallmann G., Lagos M., Michely L.T., Münker C. 2017. Redox dependent behaviour of molybdenum during magmatic processes in the terrestrial and lunar mantle: Implications for the Mo/W of the bulk silicate Moon. *Earth and Planetary Science Letters*, **474**, 503-515. https://doi.org/10.1016/j.epsl.2017.07.009

Ludwig K.R. 2012. *User's Manual for Isoplot 3.75:* A geochronological toolkit for Microsoft Excel. Berkeley Geochronology Center Special Publication No. 5. Available at: http://www.bgc.org/isoplot_etc/isoplot/Isoplot3_75-4_15manual.pdf. Accessed on: January 2020.

Marques L.S., Dupré B., Piccirillo E.M. 1999. Mantle source compositions of the Paraná Magmatic Province: evidence from trace element and Sr-Nd-Pb isotope geochemistry. *Journal of Geodynamics*, **28**(4-5), 439-459. https://doi.org/10.1016/S0264-3707(99)00020-4

Marques L.S., Rocha-Júnior E.R.V., Babinski M., Carvas K.Z., Petronilho L.A., De Min A. 2016. Lead isotope constraints on the mantle sources involved in the genesis of Mesozoic high-Ti tholeiite dykes (Urubici type) from the São Francisco Craton (Southern Espinhaço, Brazil). *Brazilian Journal of Geology*, **46**(Suppl. 1), 105-122. https://doi.org/10.1590/2317-4889201620150010

McDonough W.F., Frey F.A. 1989. Rare earth elements in upper mantle rocks. In: Lipin B.R., McKay G.A. (eds.), *Geochemistry and Mineralogy of Rare Earth Elements*. Washington, D.C.: Mineralogical Society of America, p. 99-145.

McDonough W.F., Sun S. 1995. The composition of the Earth. *Chemical Geology*, **120**(3-4), 223-253. https://doi.org/10.1016/0009-2541(94)00140-4

Melluso L., Lustrino M., Ruberti E., Brotzu P., Gomes C.B., Morbidelli L., Morra V., Svisero D.P., D'Amelio F. 2008. Major- and trace-element composition of olivine, perovskite, clinopyroxene, Cr–Fe–Ti oxides, phlogopite and host kamafugites and kimberlites, Alto Paranaíba, Brazil. *The Canadian Mineralogist*, **46**(1), 19-40. https://doi.org/10.3749/canmin.46.1.19

Meyer H.O.A., Svisero D.P. 1991. Limeira and Indaiá intrusions, Minas Gerais. In: International Kimberlite Conference, 5. Araxá, Brasil. *Field Guide Book*, p. 49-55.

Meyer H.O.A., Waring M., Posey E.F. 1991. Diamond deposits of the Santo Inácio river and the Vargem intrusions, near Coromandel, Minas Gerais. In: International Kimberlite Conference, 5. Araxá, MG, Brasil. *Field Guide Book*, p. 50-57.

Milani E.J. 1997. *Evolução tectono-estratigráfica da Bacia do Paraná e seu relacionamento com a geodinâmica fanerozóica do Gondwana Sul- Ocidental*. Ph.D. Thesis, Universidade Federal do Rio Grande do Sul, Porto Alegre, 255 p.

Mitchell R.H. 1995. *Kimberlites, Lamproites, and Related Rocks*. New York: Plenum, 410 p.

Mitchell R.H., Bergman S.C. 1991. *Petrology of lamproites*. New York: Plenum, 447 p.

Morbidelli L., Gomes C.B., Brotzu P., D'Acquarica S., Garbarino C., Ruberti E., Traversa G. 2000. The Pariquera Açu K-alkaline complex and southern Brazil lithospheric mantle source characteristics. *Journal of Asian Earth Science*, **18**(2), 129-150. https://doi.org/10.1016/S1367-9120(99)00028-0

Morimoto N., Fabries J.A., Ferguson A.K., Ginzburg I.V., Ross M., Seifert F.A., Zussman J., Aoki K., Gottardi G. 1988. Nomenclature of pyroxenes. *Mineralogical Magazine*, **52**(367), 535-550. https://doi.org/10.1180/minmag.1988.052.367.15

Nickel K.G., Green D.H. 1985. Empirical geothermobarometry for garnet peridotites and implications for the nature of the lithosphere, kimberlites and diamonds. *Earth and Planetary Science Letters*, **73**(1), 158-170. https://doi.org/10.1016/0012-821X(85)90043-3

Nimis P. 1998. Evaluation of diamond potential from the composition of peridotitic chromian diopside. *European Journal of Mineralogy*, **10**(3), 505-519.

Nowell G.M., Pearson D.G., Bell D.R., Carlson R.W., Smith C.B., Kempton P.D., Noble S.R. 2004. Hf isotope systematics of kimberlites and their megacrysts: new constraints on their source regions. *Journal of Petrology*, **45**(8), 1583-1612. https://doi.org/10.1093/petrology/egh024

Nürnberg D., Müller R.D. 1991. The tectonic evolution of the South Atlantic from late Jurassic to present. *Tectonophysics*, **191**(1-2), 27-53. https://doi.org/10.1016/0040-1951(91)90231-G

O'Neill H.St.C. 1988. System Fe–O and Cu–O: thermodynamic data for the equilibria Fe–''FeO", Fe–Fe_3O_4, ''FeO"–Fe_3O_4–Fe_2O_3, and Cu–Cu_2O and Cu_2O–CuO from emf measurements. *American Mineralogy*, **173**(5-6), 470-486.

O'Neill H.St.C., Wall V.J. 1987. The olivine–orthopyroxene–spinel oxygen geobarometer, the nickel precipitation curve, and the oxygen fugacity of the Earth's upper mantle. *Journal of Petrology*, **28**(6), 1169-1191. https://doi.org/10.1093/petrology/28.6.1169

Peate D.W., Hawkesworth C.J., Mantovani M.S.M., Rogers N.W., Turner S.P. 1999. Petrogenesis and stratigraphy of the high-Ti/Y Urubici magma type in the Paraná flood basalt province and implications for the nature of 'Dupal'-type mantle in the South Atlantic region. *Journal of Petrology*, **40**(3), 451-473. https://doi.org/10.1093/petroj/40.3.451

Philipp R.P. 1991. Geologia dos granitóides da região de Monte Bonito, Pelotas, RS: uma contribuição ao reconhecimento estratigráfico do Setor Oriental do Escudo Sul Riograndense. *Acta Geológica Leopoldensia*, **24**, 71-128.

Princivalle F., Salviulo G., Marzoli A., Piccirillo E.M. 2000. Clinopyroxene of spinel-peridotite xenoliths from Lake Nji (Cameroon Volcanic Line, WAfrica): crystal chemistry and petrological implications. *Contributions to Mineralogy and Petrology*, **139**(5), 503-508. http://dx.doi.org/10.1007/s004100000151

Princivalle F., Secco L., Demarchi G. 1989. Crystal chemistry of clinopyroxene series in ultramafic xenoliths from northeastern Brazil. *Contributions to Mineralogy Petrology*, **101**, 131-135. https://doi.org/10.1007/BF00375300

Provenzano C.A.S. 2016. *Caracterização petrográfica, química mineral e petrogênese do kimberlito Alfeu I- Canguçu/RS e uma revisão conceitual de magmatismo e rochas kimberlíticas*. Dissertação (Mestrado), Universidade Federal do Rio Grande do Sul, Porto Alegre, 215 p.

Reguir E.P., Chakhmouradian A.R., Halden N.M., Malkovets V.G., Yang P. 2009. Major- and trace-element compositional variation of phlogopite from kimberlites and carbonatites as a petrogenetic indicator. *Lithos*, **112**(Suppl. 1), 372-384. https://doi.org/10.1016/j.lithos.2009.05.023

Ribeiro M. 1980. Geossuturas do Escudo do Rio Grande do Sul. In: Congresso Brasileiro de Geologia, 31. *Anais*... Balneário Camboriú, 5, p. 2709-2718.

Rocha-Júnior E.R.V., Marques L.S., Babinski M., Nardy A.J.R., Figueiredo A.M.G., Machado F.B. 2013. Sr-Nd-Pb isotopic constraints on the nature of the mantle sources involved in the genesis of the high-Ti tholeiites from northern Paraná Continental Flood Basalts (Brazil). *Journal of South American Earth Sciences*, **46**, 9-25. https://doi.org/10.1016/j.jsames.2013.04.004

Rocha-Júnior E.R.V., Puchtel I.S., Marques L.S., Walker R.J., Machado F.B., Nardy A.J.R., Babinski M., Figueiredo A.M.G. 2012. Re-Os isotope and highly siderophile element systematics of the Paraná Continental Flood Basalts (Brazil). *Earth and Planetary Science Letters*, **337**, 164-173. https://doi.org/10.1016/j.epsl.2012.04.050

Rohrbach A., Schmidt M.W. 2011. Redox freezing and melting in the Earth's deep mantle resulting from carbon-iron redox coupling. *Nature*, **472**(7342), 209-212. https://doi.org/10.1038/nature09899

Santos J.O.S., Chernicoff C.J., Zappettini E.O., McNaughton N.J., Hartmann L.A. 2019. Large geographic and temporal extensions of the Río de la Plata Craton, South America, and its metacratonic eastern margin. *International Geology Review*, **61**(1), 56-85. https://doi.org/10.1080/00206814.2017.1405747

Schulze D.J. 2003. A classification scheme for mantle-derived garnet in kimberlite: a tool for investigating the mantle and exploring for diamonds. *Lithos*, **71**(2-4), 195-213. https://doi.org/10.1016/S0024-4937(03)00113-0

Scott Smith B.H., Nowicki T.E., Russell J.K., Webb K.J., Mitchell R.H., Hetman C.M., Robey J.V. 2018. *A Glossary of Kimberlite and Related Terms*. North Vancouver, B.C.: Scott-Smith Petrology Inc.

Shchukina E.V., Agashev A.M., Shchukin V.S. 2019. Diamond-Bearing Root Beneath the Northern East European Platform (Arkhangelsk Region, Russia): Evidence from Cr-Pyrope Trace-Element Geochemistry. *Minerals*, **9**(5), 261. https://doi.org/10.3390/min9050261

Shu Q., Brey G.P., Pearson D.G. 2018. Eclogites and garnet pyroxenites from Kimberley, Kaapvaal craton, South Africa: their diverse origins and complex metasomatic signatures. *Mineralogy and Petrology*, **112**(1), 43-56. https://doi.org/10.1007/s00710-018-0595-6

Skuzovatov S., Shatsky V.S., Ragozin A.L., Smelov A.P. 2022. The evolution of refertilized lithospheric mantle beneath the northeastern Siberian craton: Links between mantle metasomatism, thermal state and diamond potential. *Geoscience Frontiers*, **13**(6), 101455. https://doi.org/10.1016/j.gsf.2022.101455

Stagno V., Ojwang D.O., McCammon C.A., Frost D.J. 2013. The oxidation state of the mantle and the extraction of carbon from Earth's interior. *Nature*, **493**(7430), 84-88. https://doi.org/10.1038/nature11679

Svisero D.P., Chieregati L.A. 1991. Contexto geológico de kimberlitos, lamproítos e ocorrências diamantíferas do Brasil. *Boletim IG-USP*, (9), 75-81. https://doi.org/10.11606/issn.2317-8078.v0i9p75-81

Titterington D.M., Halliday A.N. 1979. On the fitting of parallel isochrons and the method of maximum likelihood: *Chemical Geology*, **26**(3-4), 183-195. https://doi.org/10.1016/0009-2541(79)90045-7

Turner S., Regelous M., Kelley S., Hawkesworth C.J., Mantovani M. 1994. Magmatism and continental break-up in the South Atlantic: high precision 40Ar-39Ar geochronology. *Earth and Planetary Science Letters*, **121**(3-4), 333-348. https://doi.org/10.1016/0012-821X(94)90076-0

Van Achterbergh E., Ryan C.G., Jackson S.E., Griffin W.L. 2001. Data reduction software for LA-ICP-MS: appendix. In: Sylvester P.J. (ed.), *Laser Ablation –ICP-Mass Spectrometry in the Earth Sciences:* Principles and Applications. Ottawa: Mineralogical Association of Canada Short Course Series, v. 29, p. 239-243.

Wijbrans C.H., Klemme S., Berndt J., Vollmer C. (2015). Experimental determination of trace element partition coefficients between spinel and silicate melt: the influence of chemical composition and oxygen fugacity. *Contributions to Mineralogy and Petrology*, **169**(4), 45. https://doi.org/10.1007/s00410-015-1128-5

Workman R.K., Hart S.R. 2005. Major and trace element composition of the depleted mantle MORB mantle (DMM). *Earth and Planetary Science Letters*, **231**(1-2), 53-72. https://doi.org/10.1016/j.epsl.2004.12.005

York D. 1969. Least-squares fitting of a straight line with correlated errors. *Earth and Planetary Science Letters*, **5**, 320-324. https://doi.org/10.1016/S0012-821X(68)80059-7

Zhao D., Esse E.J., Zhang Y. 1999. An oxygen barometer for rutile-ilmenite assemblages: oxidation state of metasomatic agents in the mantle. *Earth and Planetary Science Letters*, **166**(3-4), 127-137. https://doi.org/10.1016/S0012-821X(98)00281-7

Zi J.W., Cawood P.A., Fan W.M., Tohver E., Wang Y.J., McCuaig T.C. 2012. Generation of Early Indosinian enriched mantle-derived granitoid pluton in the Sanjiang Orogen (SW China) in response to closure of the Paleo-Tethys. *Lithos*, **140-141**, 166-182. https://doi.org/10.1016/j.lithos.2012.02.006